POLITECNICO
MILANO 1863

SCUOLA DI INGEGNERIA INDUSTRIALE
E DELL'INFORMAZIONE

Investigating Visibility for the Development of Fog Attenuation Models Affecting FSO Links

Tesi di Laurea Magistrale in
Telecommunication Engineering - Ingegneria Delle Telecomunicazioni

Author: **Paolo Volpe**

Student ID: 988529
Advisor: Prof. Lorenzo Luini
Co-advisors: Dr. Laura Resteghini
Academic Year: 2021-22

Abstract

With the ever-growing need for data and radio frequency spectrum getting overcrowded, Free Space Optics (FSO) may find a place for circumstances where fiber is too costly or excessively difficult to install. FSO is a multi-disciplinary area that draws from radio and fiber communication and it has experienced significant advances in the course of the most recent three decades.

Among the problems associated with this technology are mostly adverse weather events such as rain and fog. Current models adopted in the study of such phenomena lack standardization at the wavelength ($\lambda = 1.55\mu$m) considered in today's FSO links.

The possibility of statistically estimating adverse atmospheric events, which condition the reliability of the system, through the use of databases would further enhance the possibility of engineering transmission systems in different locations where the necessary instrumentation for measurements might not be available or uninstallable. The databases involved in the visibility analysis are: European Centre for Medium-Range Weather Forecasts (ECMWF), the Wyoming database and the visibilimeters installed on the campus of the Politecnico di Milano. The visibility can be classified according to the period and place where it is measured or analysed.

This work focuses on attenuation measurements due to visibility phenomenon. The attenuation obtained from the data analysis can be formalised using a new model that is able to incorporate spatial correlation of the visibility phenomenon and provide valuable support for the realisation of terrestrial FSO links over short distances. The new model will take into account a path reduction factor able to estimate the attenuation along the link in a more accurate way.

Keywords: Free Space Optics, Visibility, Attenuation, Spatial Correlation, Path Reduction Factor, ECMWF

Abstract in lingua italiana

Con la crescente necessità di dati e l'affollamento dello spettro delle radiofrequenze, il Free Space Optics (FSO) potrebbe trovare spazio nelle circostanze in cui la fibra sia troppo costosa o troppo difficile da installare. L'FSO è un'area multidisciplinare che attinge alle comunicazioni radio e in fibra e ha registrato progressi significativi nel corso degli ultimi tre decenni. Tra le problematiche associate a questa tecnologia ci sono per lo più eventi atmosferici avversi come pioggia e nebbia. I modelli attuali adottati nello studio di tali fenomeni mancano di standardizzazione alla lunghezza d'onda ($\lambda = 1.55\mu$m) considerata negli odierni sistemi FSO.
La possibilità di stimare statisticamente gli eventi atmosferici avversi, che condizionano l'affidabilità del sistema, tramite l'uso di database accrescerebbe ulteriormente la possibilità di ingegnerizzare sistemi di trasmissione in diverse località dove la strumentazione necessaria alle misurazioni potrebbe essere non reperibile o installabile. I database coinvolti nell'analisi della visibilità sono: European Centre for Medium-Range Weather Forecasts (ECMWF), il database del Wyoming e i visibilimetri installati presso il campus del Politecnico di Milano. La visibilità può essere classificata in base al periodo e luogo dove viene misurata o analizzata.
Questo lavoro si focalizza sulle misure di attenuazione dovute al fenomeno della visibilità. L'attenuazione ottenuta dall'analisi dei dati può essere formalizzata utilizzando un nuovo modello in grado di incorporare la correlazione spaziale del fenomeno della visibilità e di fornire un valido supporto per la realizzazione di collegamenti FSO terrestri su brevi distanze. Il nuovo modello terrà conto di un fattore di riduzione del percorso del link, il quale ci permetterà di stimare l'attenuazione lungo il collegamento in modo più accurato.

Parole chiave: Free Space Optics, Visibilità, Attenuazione, Correlazione Spaziale, Path Reduction Factor, ECMWF

Contents

Introduction

Free Space Optics (FSO) is becoming an increasingly essential technology in terrestrial communications due to the many obtainable advantages. The increasing bandwidth demand in the communication sector makes FSO, mostly in short path links, a valid alternative to the already known telecommunication systems [8], due to its utilization of a wide unlicensed spectrum. An essential point is the quite simple implementation of the FSO link, that is one of the reason why this technology is mostly used in areas where fiber links are not physically feasible. Typically this technology works in infrared band and it is capable of trasmitting tens of Gbps (Gigabits per second) over several kilometers in clear sky conditions. On the other hand FSO propagation is subjected to strong atmospheric attenuation inevitably. Some of these visibility impairments, also known as fog, rain and snow can heavily degrade the quality of service of our network infrastracture [8]. As a consequence many propagation models based on visibility phenomenon have been developed in order to predict the impact of atmospheric attenuation, various path loss models, depending on visibility, offer an analytical approach. Until today the most used technologies to detect atmospheric impairments have been instruments such as visibilimeters and rain gauges which provided the essential data to analyse in order to predict this kind of attenuation. This study investigates the possibility to use a worldwide database, ECMWF, containing visibility data which are the result of predictions based on mathematical models. This could make real the possibility of knowing in each world's locations how to model our link taking into account the visibility phenomenon. Once we understand where to find the necessary data for our model, we will analyse the various facets of the phenomenon in question, trying to understand how visibility can be conditioned by the climate and by the period in which it is measured. Afterwards we will introduce a new path reduction factor for fog phenomenon.

1 | Free Space Optics technology

In the following chapter the free space optic (FSO) system and its main aspects will be examinated. Afterwards some impairments on the link will be analysed, going into details in the concept of visibility and the estimation of attenuation in meteorological events such as fog and rain finally attenuation models proposed by the International Telecommunication Union (ITU) and Politecnico di Milano will be detailed.

1.1. An overview of FSO links

The "last mile bottleneck", or rather "connectivity bottleneck", is caused by the need for high bandwidth in metropolitan networks with short timelines, as well as the requirement for cost-effectiveness and flexibility in service provisioning (some connections being temporary, and some long term), it is not only the last mile that suffers from this issue but it is a problem which pervades metropolitan networks.
This "connectivity bottleneck" can be addressed from a technological standpoint with a few alternatives, though whether these make economic sense is a different matter. The most evident solution for the bandwidth shortage is fiber, which is undoubtedly the most reliable method of optical communication yet, but digging and the costs associated with laying the fiber, as well as the amount of time it takes to set up, are restrictive factors. Furthermore, once the fiber is laid, it becomes a sunk cost, making it almost impossible to recover if the customer leaves. Despite its technological superiority compared to free-space optics, fiber is much more expensive.
A second option is radio frequency (RF). This technology is mature and has already been deployed, but requires large investments to acquire the spectrum licenses, and cannot scale to the same optical capacities. Nevertheless, RF-based networks can cover longer distances.
The most valid alternative is free space optics (FSO). FSO is the optimum solution in terms of technology (optical) as well as bandwidth scalability, deployment speed (hours instead of months) and cost-effectiveness (at least a fifth)[14]. Free-space optics involves the transmission of optical signals through a medium with no physical connection. This

transmission, which is carried out with transmission of photons, can be done via LEDs or lasers (light amplification by stimulated emission of radiation). FSO is comparable to optical transmission over fiber-optic cables, but instead of glass, air is utilized. Interestingly enough, light moves faster through air (approx. 300,000 km/s) than it does through glass (approx. 200,000 km/s), so free-space optical communications could be considered optical communication at the speed of light.
Moving our focus on the technical mechanism behind the FSO technology it is fundamental to highlight the operational wavelength (frequency) used for our purpose which is around 1.550 μm (193 THz). Moreover that does not exclude the possibility of finding commercial FSO devices with a wavelength range between 850 and 1.550 μm, thus a group of wavelengths close to the visible spectrum and the infrared (IR) one. The two wavelengths aforesaid fall in a spectral region that do not undergo much absorption from the surrounding atmosphere. Due to the usage of this wavelengths in fiber-optic communications, the industry standard elements at the transmitter and receiver are usable too. The Federal Communications Commission (FCC) does not control the use of frequencies above 300 GHz. Therefore, unlike most microwave systems with lower frequencies, such as LMDS (Local Multipoint Distribution Service) , FSO communication systems do not need to have an operating license. Since the wavelengths in the near infrared spectrum are close to the visible spectrum, they have nearly identical propagation characteristics as visible light [14].
In order to be more accurate we are going to highlight the different implementations available for the FSO systems, therefore we can distinguish an intersatellite communication system, a lasercom, which makes possible the connection between the satellite and ground station, and the terrestrial one. Each of them has some common elements, the effective difference is the medium where the communication occurs:

FSO in Inter-Satellite links

In recent years, the space-based Internet communication system based on Low Earth Orbit (LEO) satellite constellations has become an increasingly popular technology. Several companies, such as SpaceX and Amazon, have proposed their own large constellations to provide global Internet access. Since the coverage of a single LEO satellite is limited, the Inter-Satellite Link (ISL) has become an effective way to extend the service area and reduce reliance on terrestrial infrastructure [10]. A LEO is an orbit around Earth with a period of 128 minutes or less, most of the artificial objects in space are located within this orbit, with a maximum altitude of one-third of Earth's radius.The LEO region is also known as the area of space below an altitude of 2,000 km. A LEO demands

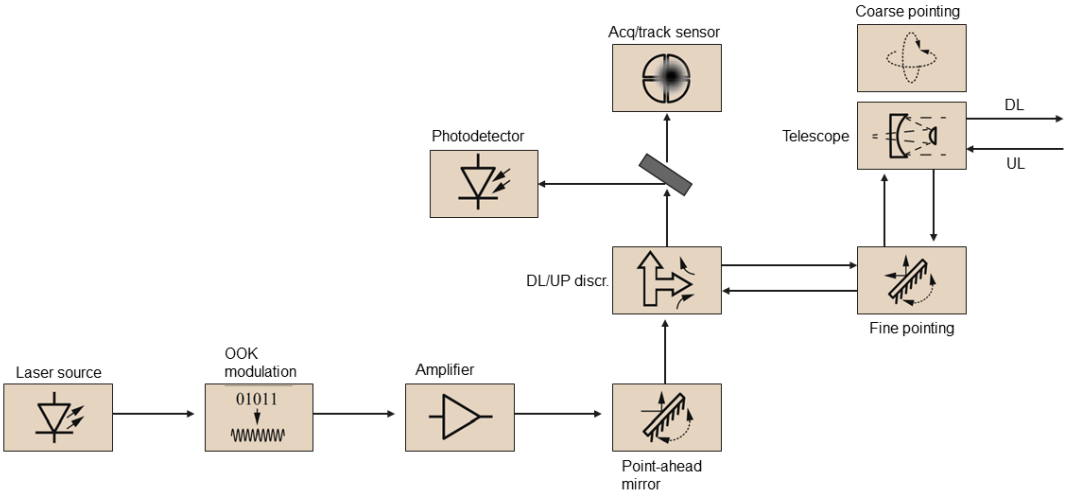

Figure 1.1: Basic diagram of the optical head assembly in a typical LEO lasercom terminal.

the least energy for satellite placement. It provides high bandwidth and low latency communication. Satellites and space stations in this orbit are far more accessible for crew and servicing [20].

Lasercom links

In lasercom links the working principle is quite the same of the latter discussed in the previous subsection. The most significant implementation of lasercom from Low Earth Orbit (LEO) is ground-to-direct downlinks, as the main purpose is to download to the Earth the ever-growing quantity of data that remote-sensing missions necessitate. The detail of these sensors is progressing steadily, thus needing even more bandwidth. In addition, with the broadening accessibility of launches to LEO, spacecraft are becoming miniaturized, such as CubeSats and other small satellites, and with multiple plans for constellations, the amount of data that will be needed to be transmitted from LEO to Earth is anticipated to erupt in the future. A regular Low Earth Orbit (LEO) lasercom terminal mainly consists of an optical head assembly and an electronics/processing assembly. As illustrated in Fig.1.1, it usually contains a telescope to broadcast a collimated ray to the ground and take the uplink beam, some instrument to distinguish downlink and uplink (generally, based on wavelength, polarization or both), a laser source (with or without booster), an On-Off Keying (OOK) external modulator, a tracking detector for the up-

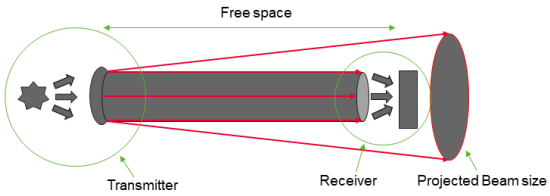

Figure 1.2: Schematic of a free-space optical transmission system.

link beacon, a fast-steering mirror for the fine-pointing and another for the point-ahead angle if necessary, a fine-pointing assembly, and optionally a fast photodetector for the communications uplink, if requested. The processing unit usually adds some codification against errors and interleaving against fading, and manages communication, telemetry, command and pointing systems [19].

FSO on terrestrial link

Free Space Optics technology on a terrestrial path is the main focus of this section. In the previous section we have introduced some concepts regarding the source of our system and the relative devices used to implement it, here our focus will be much more detailed. Starting from this fundamental assumption: in a basic point-to-point transmission system, the main goal is to set an unobstructed LOS (line-of-sight) link between the two networking locations. Fig.1.2 shows a simple schematic of a FSO transmission system [14]. The optical equipment involved at the transmitter is a light source (Laser or LED) and a telescope assembly. The role of telescope is to focus the beam onto the receiver. The beam divergence phenomenon must be taken into account, due to this latter the beam of the light source can experience a considerable change in trajectory as consequence the beam arrives not well collimated at receiver or in worst cases it does not focus the receiver properly. The transmitted light is accepted at the receiver end by utilizing a lens or a mirror. Afterward, the acquired light is concentrated on a photodetector. In all realistic cases, the projected beam size at the receiving end is significantly bigger than the size of the receiving optics. Thus, some of the transmitted light is lost during the transmission

process. Depending on the actual beam divergence, the projected beam size can be several meters, while the typical diameter of the receiving telescope is more likely to be 8-20 cm. This phenomenon is recognized as geometrical path loss. The utilization of a tighter beam decreases the amount of geometrical path loss. Nevertheless, narrow beams necessitate a very reliable mounting platform or an even more complex active beam-tracking system [14].

Transmitter

In modern FSO systems, a variety of light sources are employed for the transmission of optical data. We will concentrate on semiconductor-based transmission sources since semiconductor lasers are presently the principal transmission media in commercial FSO systems. The major distinctions between these transmission sources are wavelength, power, and modulation rate. The cost for a high-performance transmitter can range from tens to thousands of dollars. The selection of a particular transmission source is determined by the particular target application [14].

Light-Emitting Diodes (LED): A light-emitting diode (LED) is a semiconductor *pn junction*. It is a device that emits light when an external forward-bias voltage is applied. Electrons in the semiconductor join with electron holes, generating energy in the form of photons. The colour of the light (corresponding to the energy of the photons) is dictated by the energy needed for electrons to cross the band gap of the semiconductor. It became available as practical electronic components in 1962, the earliest LEDs emitted low-intensity infrared (IR) light [12]. Due to their relatively low transmission power, LEDs are usually applied in applications over shorter distances with moderate bandwidth requirements up to 155 Mbps. Depending on the material system, LEDs can operate in various wavelength ranges. When compared to narrowband (or single wavelength) laser transmission sources, LEDs have a much larger spectral range of operation [14].

Laser: In the past paragraph we dealt with the importance of the transmitter in order to perform the link properly. Laser is the most used technology in FSO, typically in infra-red (IR) region. The function mechanism is similar to the LED but with somewhat different both in how it works and its characteristics. Laser stands for Light Amplification by Stimulated Emission of Radiation, this theory was introduced by Albert Einstein around 1916 anyway the first demonstration of a solid state ruby laser was performed in 1960 at IBM while in 1961 a Bell Labs helium-neon laser demonstration took place. In laser device some phenomena must be take into account such as the beam divergence: the spreading of the beam is an angle measure of the widening of the beam size or radius as it moves away from the optical opening from which it originates; the scattering of light caused by microscopic particles and/or irregularities on the surface happens, to some

extent, every time light interacts with matter and is the main reason why a laser beam with good collimation can be seen when it passes through the air or is reflected by a mirror. Generally, the amount of scattered light increases in relation to the concentration of particles in a mass and to the "roughness" of a surface [14].

Receiver

In addition to transmission sources, light detectors are an important element of the FSO system's design. Light receivers detect light by exploiting different physical effects. Similarly to laser sources, most detectors used in commercial FSO systems are based on semiconductors. Depending on the specific material system, they can work in different wavelength ranges. Most common photodetector are the PIN and Avalanche photodiode, the latter differs from the first due to the intrisic gain that they can add to the detected signal. In modern applications for high-speed communications, two fundamental physical mechanisms are used to detect light signals: the external and the internal photoelectric effect. Both of them convert the energy of the incoming photons into electrical energy. Vacuum diodes or photomultipliers rely on the external photoelectric effect, while semiconductor detectors such as PIN or Avalanche diodes use the internal photoelectric effect to detect photons. Some important factors such as responsivity and spectral response are the main reference parameters in order to test the reliability of the photodetector [14].

Optical Subsystem

Optical subsystems have an essential role in the design of an FSO system. Optical components are employed both on the transmission and receiver side of an optical link. In contemporary FSO systems, different designs based on lenses and mirrors are used. Lenses are based on the physics of light refraction, while mirrors are based on the reflective properties of materials. The design selected often depends on the performance requirements for the specific application and the available cost [14].

1.2. Impairments in FSO link on terrestrial path

The biggest challenge for FSO is given by the propagation impairments such as fog, rain, snow and turbulance that can be considered as the most significant sources of signal fade across terrestrial FSO links. Fog and rain, specifically, can cause severe propagation loss which reduce the availability of the terrestrial optical links,impact on the maximum path length for a system that needs high-availability. This phenomena are linked to the optical channel wavelength, which is normally around 1.55 μm, due to its compliance with eye-safety regulations and the cheaper hardware's cost. Recent studies[21] show a reduced effect of the fog in the 10 μm band, making the interest in the lower optical

growing frequencies. Given the potential application of FSO in mobile networks, there is a requirement for basic and broad-reaching channel models. Differently from the clearly established ITU-R recommendations which provide methods for predicting propagation issues at mmWaves frequency, there is a lack of standardization in the FSO field. In this chapter we are going to analyse the different propagation models from the state of the art literature [21].

1.2.1. Visibility general definition

The literature emphasizes the disparities between different $\gamma - V$ models based on different characteristics: employed technique and definition of visibility. Initially, visibility should be defined according to an unbiased law. Adhering to the WMO recommendations, visibility is equal to the Meteorological Optical Range (MOR)[21], which is defined as the distance the light from a 2700 K incandescent lamp has to travel through the atmosphere before the intensity drops to 0.05 of its original value. Color temperature (Kelvin) of a light source is the absolute temperature of an ideal black-body radior that radiates light of a color comparable to that of the light source. The irradiance propagation through a uniform layer of particles follows an exponential decay behaviour, as predicted by the Bourguer-Lambert law. We are able to derive the relationship between γ (dB/km) and V(km) [21].

$$\gamma = \frac{13}{V} \tag{1.1}$$

It is useful to introduce some concepts about scattering phenomena in order to well explain the physics behind the following theory. When the laser beam of the transmitter travels trough the fog or whatever type of meteorological phenomena aforementioned before, it is affected by scattering. Scattering is the process of absorption and then re-emission of light energy. In scattering, light spreads in all directions. The air molecules of size smaller than the wavelength of incident light absorb the energy of incident light and re-emit it without change in its wavelength. In order to distinguish which type of scattering our signal is experiencing we can summarise it in the Fig.1.3. In this figure we can appreciate the different scattering phenomena. They are function of molecules size and λ. Grwoing in molecules size we move from Rayleigh to geometrical scattering.
The λ^4 dependence and the size of particles present in the atmosphere suggest that shorter wavelengths are scattered more than longer wavelengths. However, for FSO systems that work in the near infrared range or longer wavelengths, the effect of Rayleigh scattering on the transmission signal can be ignored [14].
Rayleigh scattering refers mainly to the elastic scattering of light from particles of atomic

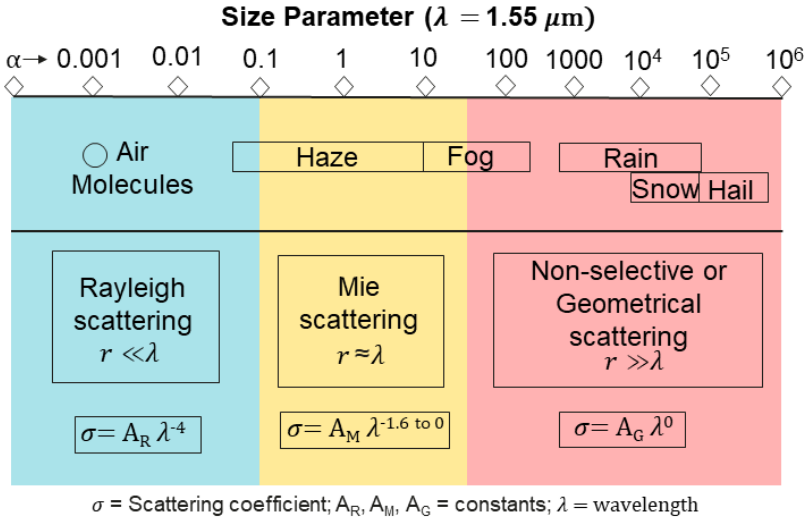

Figure 1.3: Scattering Phenomena

and molecular size whose diameter is lower than around one-tenth of the wavelength of the incoming light. Mie scattering refers mainly to the elastic scattering of light from particles of atomic and molecular size whose diameter is greater than around the wavelength of the incoming light. Therefore, in the near infrared wave length range, particles of fog, haze and pollution (aerosols) are the main contributors to the Mie scattering process. This theory is complicated but well comprehended. For aerosols, this distribution depends on place, time, relative humidity, wind speed, and so on. A simple empirical formula, found in literature (ITU-R P.1814)[15] and that is broadly used in the FSO society to calculate the attenuation coefficient due to Mie scattering, is given by the following:

$$\gamma = \frac{K}{V}\left(\frac{0.550}{\lambda}\right)^{q} \qquad q = \begin{cases} 1.6, & V > 50\ km \\ 1.3, & 6\ km < V \leq 50\ km \\ 0.585V^{\frac{1}{3}}, & V < 6\ km \end{cases} \tag{1.2}$$

The visibility is expressed as V, while k depends on the measured method shown in table1.1 , λ is the wavelength in μm and q depends on V. The transmission wavelength dependence of the attenuation coefficient γ does not follow the predicted empirical for-

Table 1.1: Recommended value of the coefficient K [21]

Visibility Observation Method		
K	**Measured method**	**Inaccuracy**
9.6	Observation evaluated by visual method of the light source at night	40%
11.3	Observation evaluated by visual method of a black object against the shy horizon during the morning	22%
13.0	MOR measurement by means of technical instrumentation	5-20%
$-4.34 \ln T$	Measurement by means of technical instrumentation of visibility, where T describes the irradiance	

mula. More accurate numerical simulations of the exact Mie scattering formula propose that the attenuation coefficient does not vary a lot with the wavelength so long as the near infrared wavelength range typically used in FSO systems is concerned. The overall outcome that can be drawn from empirical observation is that Mie scattering caused by fog characterizes the primary source of beam attenuation, and that this effect is accentuated as distance is increased. For all practical purposes, the visibility conditions in the FSO deployment area must be studied [21].

1.2.2. Attenuation due to fog (Mie Scattering)

Fog is a thick cloud of tiny water droplets that forms near ground level and can cause horizontal visibility to fall below 1 km. The term "fog" can also be used to describe clouds made up of mixtures of smoke particles or ice particles. If visibility is greater than 1 km, the phenomenon is usually referred to as either mist or haze, depending on whether the obscurity is caused by water droplets or solid particles.

Fog occurs when water vapor in the air condenses onto tiny particles known as condensation nuclei, which are always present in natural air. This process happens when the relative humidity of the air exceeds saturation by even a small fraction of 1 % [6]. A fundamental parameter which helps us to describe the fog is the particle size distribution (PSD). It is the number of fog droplets per unit volume falling within a size bin, and the extinction cross section of a particle of given size. Several fog models are available: we

are going to describe the most interesting for us.

KIM Model

Fog attenuation is roughly not affected by the wavelength at least up to 1.550 μm and visibility (V) values of up to 1 km. This only applies to certain types of fog, when the DSD changes a lot, the attenuation also changes. When V and/or the wavelength increase, γ becomes less tied to V , depending on the type of fog. In this respect, recent data on fog microphysics reveal multimodal PSD shapes, which in turn cause a more marked wavelength selective behavior than predicted by classical fog models.
KIM model is an evolution of Kruse model, to be used also when the visibility value is lower than 6 km and it is valid for $0.4\mu m \leq \lambda \leq 1.55\mu m$.:

$$\gamma = \frac{17}{V}(\frac{0.550}{\lambda})^q \qquad q = \begin{cases} 1.6, & V > 50\ km \\ 1.3, & 6\ km < V \leq 50\ km \\ 0.16V + 0.34, & 1\ km \leq V \leq 6\ km \\ V - 0.5, & 0.5\ km \leq V \leq 1\ km \\ 0, & V < 0.5\ km \end{cases} \tag{1.3}$$

The inputs parameters are the following:

- V is the visibility in km
- $K = -4.34ln(T)$ where T =0.02
- λ is the wavelength in μm
- q depends on V

In Fig.1.4 it is possible to appreciate the extinction coefficient at 1.55 μm in comparison with the visibility, considering the preceding many PSDs. In this figure there is no only KIM model curve. We can notice models as function of the PSD considered distinguishing among radiation fog, haze, evaporation and so on. In the first 1 km of visibility it is clear the trend of γ, the differentiation between the curves begins for higher threshold values.

Politecnico di Milano - Upper and Lower Bound Model

The model for path loss enables quantification of key FSO link design parameters, including the maximum path length attainable. We then evaluated the impact of inaccuracies in the γ-V model on path length computation, particularly with regard to two sources of

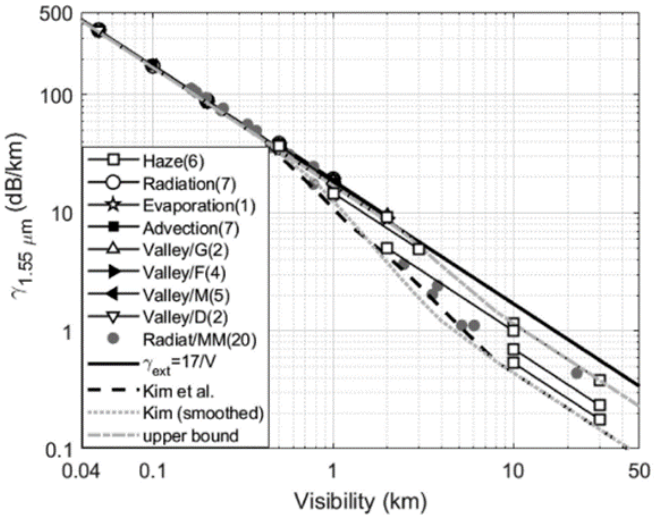

Figure 1.4: Extinction coefficient as function of the attenuation model

uncertainty in converting visibility measurements to the extinction coefficient of fog:

1. The method of measuring visibility
2. The effect of fog microphysics

Assuming fog attenuation as the primary component of atmospheric path loss, we present an abbreviated FSO power budget equation. The path loss model makes it possible to quantify fundamental FSO link design parameters such as the maximum attainable path length. The following model highlights the impact of γ-V model inaccuracy on the calculation of the path length. First of all, we should define the FSO power budget equation:

$$\gamma L - 10\log_{10}\frac{A_R}{\pi(\Theta_T L)^2} + 60 = P_T - P_R - A_{sys} \tag{1.4}$$

The quantities implied in the formula 1.4 are:

- P_T = Transmitted power [dBm]
- P_R = Received power [dBm]

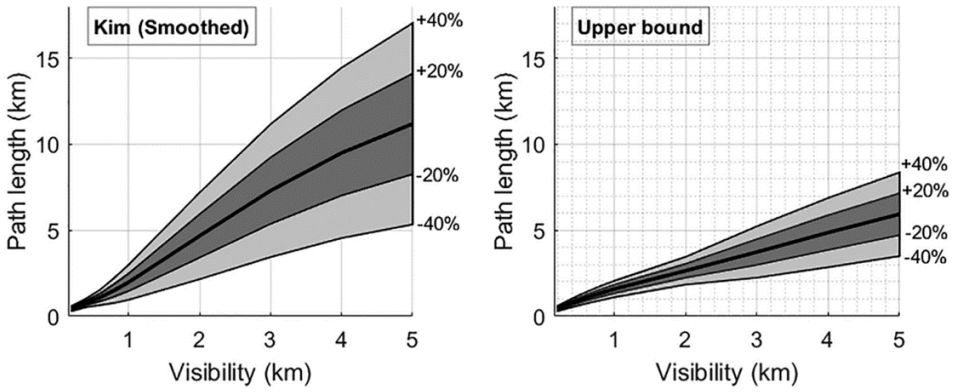

Figure 1.5: Path length as a function of the visibility across the path. Dark and light areas illustrate the relative uncertainty of the visibility measurements which could be affected of, up to 20% and 40% respectively [21]

- A_{sys} = System losses [dB]
- A_R = Receiver Area [m^2]
- Θ_T = Beam divergence [rad]
- L = Path length [km]

Differentiating the equation 1.4 we obtain:

$$\frac{dL}{L} = -\left[1 + \frac{20}{\ln 10}\frac{1}{\gamma L}\right]^{-1}\frac{d\gamma}{\gamma} \tag{1.5}$$

Lastly, the sensitivity of γ to V must be calculated, for example considering λ at 1.55 μm, by employing lower and upper bounds for γ. As the Kim model has discontinuous derivatives at the boundary points of each segment, what exactly fit this is a third-order polynomials between the low visibility segment, i.e., V $\leq$ 0.5 km and the high-visibility range, (V $\geq$ 6 km), which fits in well with the Rayleigh regime, in which the exponent q is constant. Thus

$$\gamma = \frac{p_1}{V^3} + \frac{p_2}{V^2} + \frac{p_3}{V} + p_4 \tag{1.6}$$

Imposing the continuity of the derivatives we obtain each value of p coefficients, p_1 = -4.417, p_2 = 17.783, p_3 = -1.144 , p_4 = 0.453, obtaining the lower bound model or Kim

smoothed. At the same time, we can find an upper bound, using different visibility thresholds, to fit better the outcomes of the micro-physical model. The resulting coefficients for the upper bound are: p_1 = -51.525, p_2 = 53.242, p_3 = 2.380 , p_4 = 0.429. Fig.1.5 shows the available FSO path length at 1.55 μm as a function of the visibility across the link, based on the smoothed Kim model and the upper bound model, respectively (thick black lines). Given V, γ is derived from the chosen γ-V relationship and the maximum attainable path length is calculated from (1.4) once the other system parameters are specified. The shaded areas in Fig.1.5 indicate the uncertainties due to the joint effect of the accuracy of visibility measurements and the γ-V model. The boundaries of the two shaded areas in grey correspond to 20% and 40% uncertainty bounds on V , respectively [22].

1.2.3. Attenuation due to rain (Geometrical scattering)

It is well known that some locations have higher probability of experiencing for more days per year heavy rain or thunderstorms than others. We are going to evaluate several rain attenuation prediction models that can be used for terrestrial microwave links. According to now days theory regarding rain, the attenuation estimation of this phenomenon is strictly correlated to the DSD (Drop Size Distribution) of water particles [21]. We can define the DSD, or granulometry of rain, such the distribution of the number of raindrops relative to their diameter. Three mechanisms explain the formation of drops: condensation of water vapor, assemblage of small drops on larger drops and collisions between sizes.

RECOMMENDATION ITU-R P.1814

ITU-1814 recommendation presents propagation prediction techniques for designing ground-based free-space optical systems. It features methods to quantify fading in clear atmosphere, mist, and rain and snowfall. It also encompasses scintillation and degradation caused by sunlight. Climate and in particular the local weather in the region of the chosen link path will affect the presence of snow, rain, drizzle, mist, haze, aerosol and dust/sand which will result in the absorption and diffusion of the transmitted signal[15]. Specific rain attenuation γ_{rain} (dB/km) is the following [22]:

$$\gamma_{rain} = k \cdot R^{\alpha} \tag{1.7}$$

Equation 1.7 gives the specific attenuation exceeded for the same percentage p. The parameters k and α are based on the rain characteristics, in this model k, α are estimated at 780/800 nm.

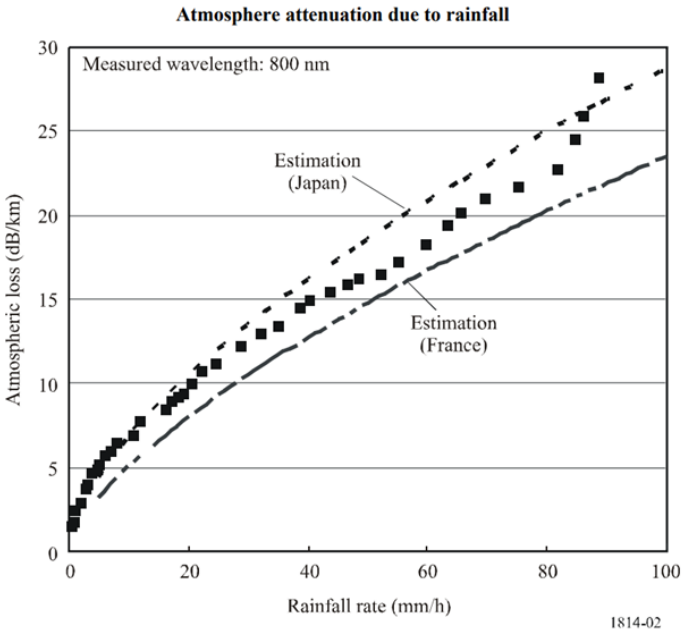

Figure 1.6: Atmosphere attenuation due to rainfall [15]

In Fig.1.6 is illustrated the relationship between γ_{rain} and rainfall rate, R, considering two locations for the parameters k and α, Japan and France respectively [15]. We can resume the inputs parameters needed for this model as follow:

- The operation frequency
- The power-law coefficients k and α for the conversion of the rain rate, R, into specific attenuation γ, consider the micro-physics of the raindrops.

Politecnico di Milano Model

This model is one of the latest formulated and we are going to analyse in this study. The specific attenuation caused by rain is not affected by the wavelength in the optical transmission windows usually employed by commercial FSO systems, such as the traditional 0.780–0.850 and 1.520–1.6 μm bands. For practical applications, the specific attenuation γ (in dB/km) is normally calculated using simple power-law relationships [22]:

$$\gamma = k \cdot R^{\alpha} \tag{1.8}$$

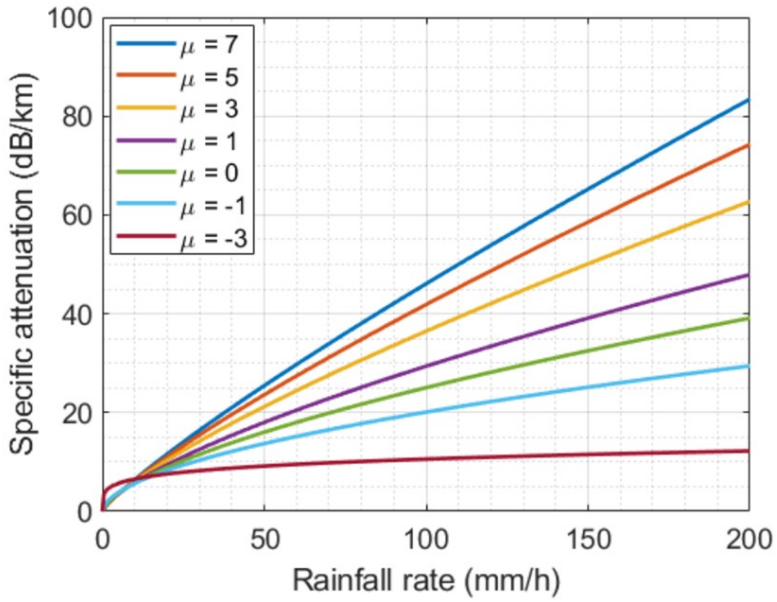

Figure 1.7: Specific attenuation due to rain against rainfall rate with various values of the shape parameter μ as indicated in Table 1.2 [21]

For this model the inputs are the following:

- R is the Rain Rate (mm/h);
- coefficients k and α, illustrated in Fig.1.7 ,are rather sensitive to the Drop Size Distribution (DSD), i.e. the particle size of the rain drops which is fundamental in order to estimate the attenuation . In case they are not available, they can be calculated with the expressions in Recommendation ITU-R P.838-3.

The total rain attenuation A(in dB) affecting the FSO link is calculated as:

$$A = \int_L \gamma(l)\, dl = \int_L k \cdot R(l)^{\alpha}\, dl \tag{1.9}$$

where L is the length of the link; k and α are the power-law coefficients and R(l) is the rain rate at position l along the path.

Path Reduction Factor Model

We introduce the concept of Path Reduction Factor, object of studies in literature regarding the attenuation due to rain. This model is an analytical technique that can be used to assess the Path Attenuation. The path reduction factor taken into consideration

Shape parameter μ	k	α
-3	4.0684	0.2077
-2	2.2838	0.4050
-1	1.5921	0.5506
0	1.2924	0.6436
1	1.1394	0.7057
2	1.0505	0.7497
3	0.9938	0.7823
4	0.9551	0.8074
5	0.9273	0.8273
6	0.9065	0.8435
7	0.8905	0.8569
8	0.8779	0.8682

Table 1.2: Coefficients α and k for multiple values of the DSD shape parameter μ [21]

to account the effect of rain variations along the propagation path and allows to estimate the path attenuation from the sole knowledge of the rain rate measured at either side of the link.
The procedure is the following:

- Calculate the path reduction factor (this is one of the possible implementable PRF case) [21], r as

$$r = \frac{1}{1 + \frac{L}{L(R)}} \tag{1.10}$$

  where L(R) can be written as:

$$L(R) = \frac{2623}{R - 6.2} \tag{1.11}$$

- Calculate the rainfall attenuation exceeded for a percentage P, where $L_{eff} = L \cdot r$:

$$A(P) = kR^{\alpha}L_{eff} = kR^{\alpha}Lr \qquad [dB] \tag{1.12}$$

Multiple scattering induced by rain drops

When an optical wave encounters a raindrop, some of the radiation is absorbed and some is scattered. In the range of wavelengths used by existing FSO systems (i.e. from 0.785 to 1.55 μm), scattering is the main phenomenon. When the particle is several times larger than the wavelength, scattering produces a narrow peak of radiation in the forward direction. Therefore, laser beam attenuation (in dB) over a path of length L in the rain

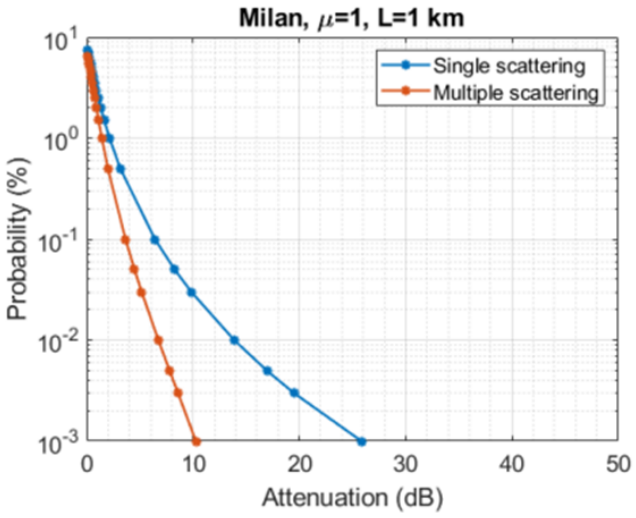

Figure 1.8: CCDF of Multiple scattering in Milano

can be expressed as [21]:

$$A_{ms}(L) = A_{rain}(L, R) - G_{ms}(L, R) \tag{1.13}$$

The inputs are:

- A_{rain} is the attenuation due to rain
- G_{ms} is the scattering gain and can be calculated as:

$$G_{ms} = aL^b \qquad [dB] \tag{1.14}$$

- The coefficient a and b are calculated according to Rain Rate R and q_n coefficients that depends from DSD:

$$a(R) = q_0 + q_1 ln(R) + q_2 [ln(R)]^2 \tag{1.15}$$

$$b(R) = q_0 + q_1 ln(R) + q_2 [ln(R)]^2 \tag{1.16}$$

In Fig.1.8 [21] is shown the CCDF of rain attenuation over a 1 km path calculated assuming single scattering and including the effects of multiple scattering for Milan in order to have a general view of this multiple scattering behaviour. From the graph we can appreciate the lower attenuation experienced by the signal due to the multiple gain scattering acquired during the propagation with respect to the single scattering curve.

1.2.4. Clear air turbulence

Apparently, with a clear sky and no meteorological events such as fog or rain we would say the total attenuation which affects our laser beam is zero, but actually this is not true and this phenomenon is called turbulence. Classical studies of turbulence focused on fluctuations in the velocity of a viscous liquid. In particular, it has been discovered that the longitudinal wind speed linked to the turbulent atmosphere randomly fluctuates around its mean value. In other words, the wind velocity field is a random or stochastic field, which means that at each point in space and time within the flow the velocity could be represented by a random variable.
Turbulence of the atmosphere caused by moisture and temperature gradients produces disturbances in the atmosphere's refractive index in the form of cells named optical turbules. Early studies by Kolmogorov suggest that a subclass of optical turbules has a statistical consistency that allows a meaningful theoretical analysis. Optical turbulence can be defined as the fluctuations in the index of refraction resulting from small temperature fluctuations. Random space-time redistribution of the refractive index causes a variety of effects on an optical wave associated with its temporal irradiance variations (scintillation) and phase fluctuations (turbulence). [16]

1.3. Thesis Objectives

The contributions of this thesis can be summarized as follows:

1. Analysis of visibility data from the ECMWF (European Center for Medium-Range Weather Forecasts) database and a validation of this latter by means of a comparison with empirical measurements from different visibilimeters belonging to different locations

   By means of the data acquired from ECMWF we will be able to compare it to the visibilimeters and NOAA (The National Oceanic and Atmospheric Administration database). In this case visibilimeter has the most accurated data regarding visibility phenomenon. The validation of ECMWF would make it reliable and dependable

for other studies and researches. Crucial thing, FSO links could be designed and installed in locations where there is no need of instrumentation or other type of devices to study meteorological phenomena.

2. Analysis of visibility behaviour under different time period and spatial locations

   Visibility is dependent on many atmospheric parameters. Recent studies [21] prove that fog, in particular, is dependent on the climate, the location and the season.

3. Statistical model of attenuation due to visibility

   Being able to statistically generalize somehow the attenuation due to visibility could be really helpful in comprehending which is its behaviour. The statistical distribution we are looking for is the most generalized possible. Moreover we identify a specific attenuation trend values. The shape of that distribution will be also classified on the database and instruments used to collect the data.

4. Analysis of spatial correlation between different locations and how much it depends on the geographical environment of the location

   Spatial correlation is always been a powerful instrument to derive specific property of a phenomenon. In this case visibility can be classified by means of this function we will be able to deduce how visibility is correlated in space. This will be analysed for both database and visibilimeters.

5. How the introduction of a Path Reduction Factor (PRF) can improve the prediction of attenuation of about 1 km optical link

   Estimating the attenuation on an optical link is the basis of this study. The contribution of a PRF would help to get a much more detailed and accurate picture than the models used so far in the infrared.

2 | Analysis of Visibility Meteorological Data

In the previous chapters, we evaluated how visibility can reduce the transmitted signal strength for an FSO link. On the other hand, visibility can also have an impact on other events. An example is the airline transportation companies. The ECMWF produces Global indicators linked to hazardous weather conditions which can lead to disruption in air travel [1]. The estimation of this event through the use of databases which contain the data obtained and processed through numerical forecasts give the possibility of having a detailed picture of a given location. Conversely, analysis using a measuring instrument can sometimes be more accurate but not always possible. We have to take into account the difficulties in installing the device and everything that comes with it. The ECMWF database stands out as a possible alternative to the instruments commonly used to measure visibility. In this chapter the main databases described will be ECWMF, NOAA and the visibilimeters available in Politecnico di Milano.

2.1. ECMWF database

Surface meteorological data have been taken from various locations. The reference database is the European Center for Medium-Range Weather Forecasts (ECMWF). ECMWF's operational forecasts seek to display how is the weather evolution in time. In order to accomplish this, the Centre generates an ensemble of predictions. Individually, they are full accounts of the evolution of the weather. Together, they indicate the probability of a range of potential future weather scenarios [4].
In order to be more accurate we are going to refer to the Meteorological Archival and Retrieval System (MARS) catalogue which is a set of data from ECMWF operational archive. Forecast working procedure is the following: ten-day forecasts on a global scale based on the 00/12 UTC Analysis, the forecast products are classified into the same categories as the data from the Analysis: Surface, Model levels, Pressure levels, and isentropic levels. Meteorological parameters are recorded at every forecast time step, with

3-hourly intervals from 00 to 72 hours, and 6-hourly from 72 to 240 hours [5]. First visibility diagnostic was introduced in the Integrated Forecasting System (IFS) cycle 41r1 at ECMWF from May 2015. The diagnosis reflects the horizontal visibility close to the surface, equivalent to the visibility information recorded in surface synoptic observations (SYNOP) messages.

The number of meteorological parameters that can have an effect on visibility, includes the presence of small droplets (fog), precipitation and aerosol. The influence of aerosol is conditioned by the environmental humidity as hygroscopic aerosol can become bigger through condensational growth, forming small haze particles. The IFS predicts water vapour, the amount of cloud liquid water, the amount of ice water, rain and snow, but it relies on a climatological variation of aerosol species (organic, sulphate, sea salt, dust, black carbon) that changes between seasons. So, in practice, the IFS is capable of reproducing the decreased visibility effects of fog, precipitation and humidity (based on a variable aerosol climatology), but not of local changes of the aerosol fields, such as considerable air pollution in high-pressure situations on land. Fog, in particular, is a weather hazard of great importance but difficult to predict. The new diagnostic includes information on the reduced visibility in fog, usually defined as visibility less than a kilometer. However, correctly predicting the emergence and disappearance of fog depends on an accurate representation of the surface characteristics (e.g. soil moisture and temperature), dynamic and thermodynamic conditions in the boundary layer and interactions with the radiation. Fog can be very variable in space and time, often linked to orographic features that the model does not resolve, so representativity errors may be locally significant, even if the mean conditions on the resolved scales of the model are predicted accurately. Given the great uncertainty in predicting fog, a probabilistic approach using the ensemble members will be more effective.

In ECMWF database visibility is expressed as function of the total extinction coefficient, β_{tot} (dB/km), considering optical wavelength in the atmosphere, and the parameter ϵ which represents the fixed liminal contrast for the visual range [13]. The visibility, V (in meter), is defined as follow:

$$V = -(\ln \epsilon)/\beta_{tot} \tag{2.1}$$

In equation (2.1) the value of ϵ is set to 0.02, a value which has been investigated and proposed by Koschmieder (1924) [17]. The overall extinction coefficient is a combination of contributions from clean air, aerosol, cloud, precipitation, and surface reflection, and it is summarized in the following fomula:

$$\beta_{tot} = \beta_{air} + \beta_{aerosol} + \beta_{cloud} + \beta_{tot} + \beta_{precip} \tag{2.2}$$

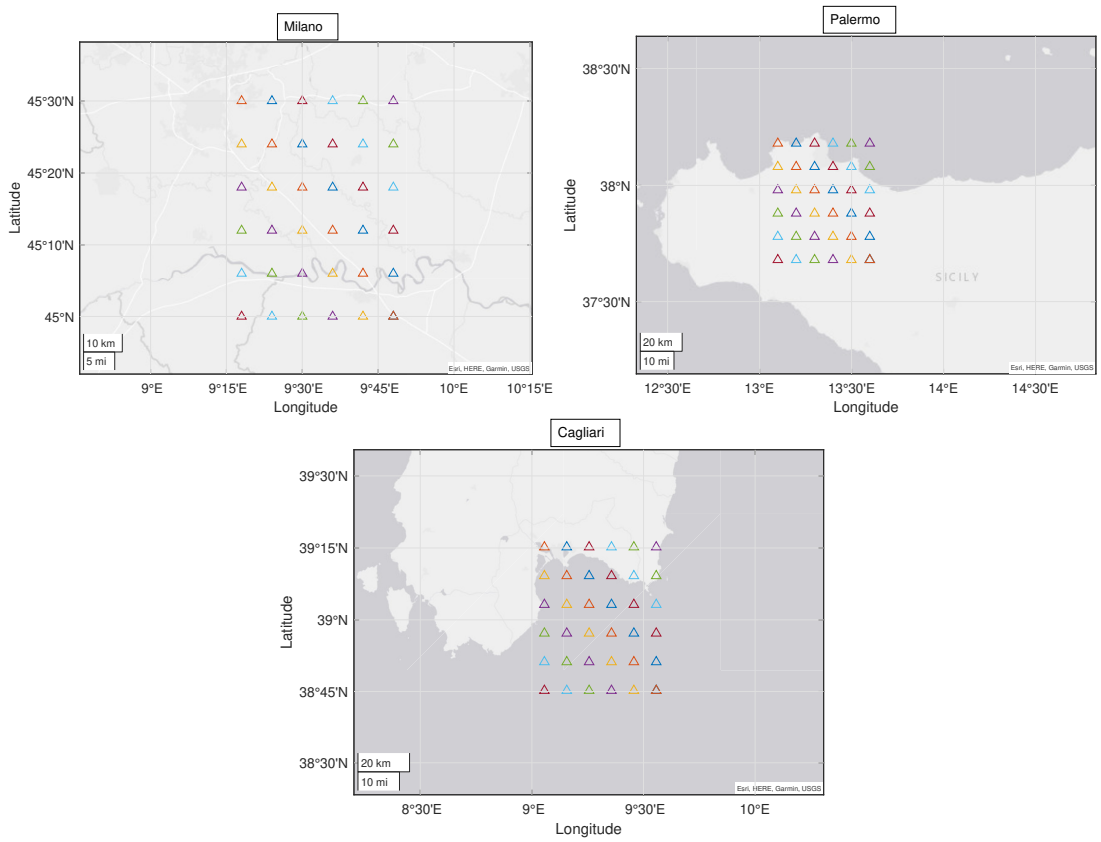

Figure 2.1: ECMWF pixel grids

The adopted procedure in order to gain the access to the ECMWF data has been the following:

1. Define a batch file for sending the request to the API (Application Programming Interface) interface of ECMWF website
2. Define the time period for which the request must be generated
3. Define each kind of characteristic of the data to be downloaded:
    - Amospheric model
    - Surface Model
    - Operational level
    - Parameter code (Visibility in our case)
4. Define the forecast time step in hours
    - For our purposes the time step is 12 hours

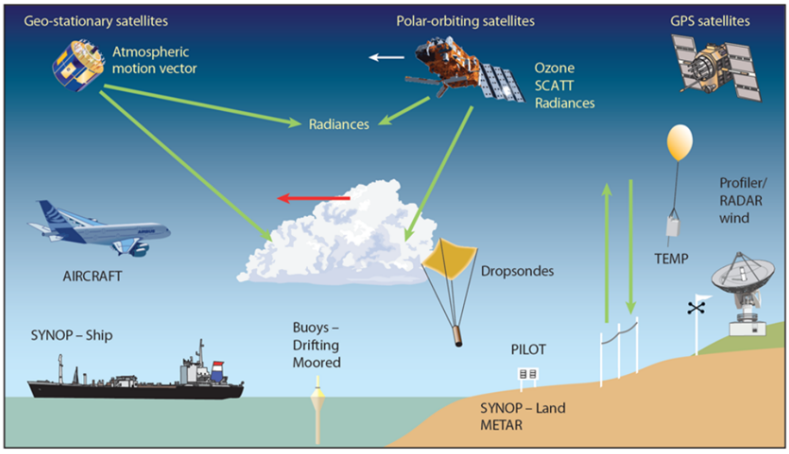

Figure 2.2: ECMWF sensors for atmospheric prediction [4]

Fig.2.2 an example of sensor used by ECMWF to detect surface data. According to ECMWF dataset we have downloaded visibility data of Milano from January 2021 up to December 2022 to be compared with visibilimeter dataset of Politecnico di Milano, while for Cagliari and Palermo only for 2021. The grid of our data is represented in Fig.2.1. The pixel analysed, which dimension is 0.1° x 0.1°, are spaced of about 10 km each other, and the grid is composed by 6x6 pixels. In Fig.2.3 are shown some time series regarding the ECMWF locations. This shows us how is the evolution in time of our visibility parameter. We can notice that maximum visibility value is 10 km, this is due to the saturation imposed on data set before the processing otherwise visibility data obtained from ECMWF are in range of 0.05-49 km. Values over 10 km are really pointless for our analysis.

2.2. Statistical Tools

Since the analyses that follow have a strong statistical component [7], it seems useful to introduce some mathematical concepts that will be used from now until the end of the chapters. First of all the analysis starts from the study of the Probability Density Function (PDF) of our visibility data. The PDF is employed to define the likelihood of the random variable taking on a particular range of values, rather than any one value. This probability is given by the integration of this variable's PDF within that range - that

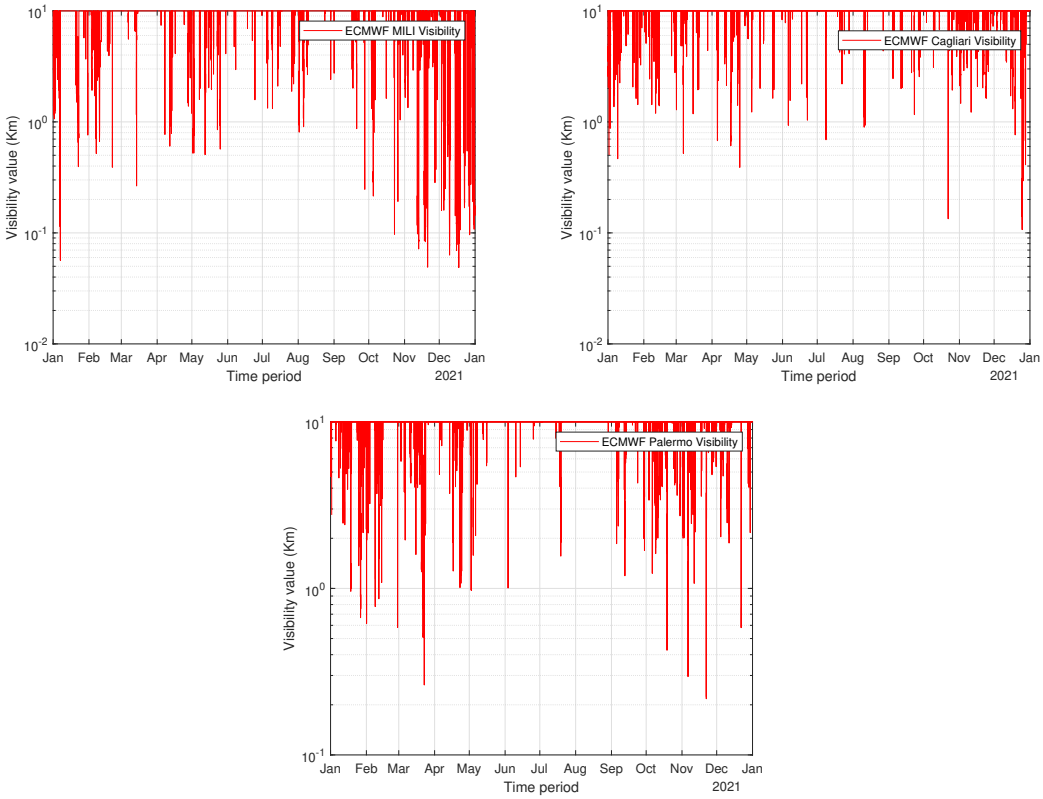

Figure 2.3: Temporal series of MILI, Palermo and Cagliari data

is, it is given by the area under the density function but above the horizontal axis and between the smallest and greatest numbers of the range. The probability density function is positive everywhere, and the area under the whole curve is equivalent to 1. From a mathematical point of view we can express our function in this way:

$$Pr[a \leq X \geq b] = \int_a^b f_X(x)dx \tag{2.3}$$

From the definition above it is possible to deduce another statistic formula which gives us another point of view of our data: the Cumulative Distribution Function (CDF).

$$F_X(x) = \int_{-\infty}^{a} f_X(u)du \tag{2.4}$$

Hence, if F_x is continuous at x we can write it as follow:

$$f_X(x) = \frac{d}{dx}F_X(x) \tag{2.5}$$

The cumulative distribution function (CDF) of a real-valued random variable X, or just the distribution function of X, evaluated at x, is the probability that X will be less than or equal to x.
Last function considered for our purposes is the Complementary Cumulative Distribution Function (CCDF) or simply the tail distribution or exceeds, which is an offshoot of the CDF. Analytically it can be written as:

$$\bar{F}_x = P(X > x) = 1 - F_X(x) \tag{2.6}$$

Due to these mathematical concepts we are able to well explain the behaviour of our data with respect to the geographical region were they have been collected and the relative time period [7].

2.3. Visibilimeter database

The visibilimeter is a precision instrument used to measure the visibility of the atmosphere. It is used to measure the atmospheric turbidity of a location, which is an indication of the concentration of particles in the air that affect visibility. It is also used to measure the amount of aerosols in the atmosphere, which can affect air quality and visibility. The device works by emitting a narrow beam of light in the visible spectrum mostly and then measuring the amount of light that is scattered back. The amount of light scattered back provides an indication of the visibility of the atmosphere. The database is built using the data collected by Politecnico di Milano in the framework of a propagation experiment within Huawei's "JointLab".

2.3.1. Politecnico di Milano - Buildings

In Milano campus there are different available visibilimeters (Fig.2.4) [11]. The buildings aforementioned, i.e. Building 24 (B24) and Casa dello Studente (CdS), have the Vaisala PWD20 visibilimeter installed [25]. It is represented in Fig.2.5. PWD20 has observation range of MOR of 10 to 20000 metres, which is suitable for most applications. With a measurement range of 10 up to 20 000 meters, PWD20 offers long range visibility measurement for different applications covering heliports, coastal areas, windmill parks – indeed, any locations or areas where visibility measurement is absolutely necessary. It operates in three modes, namely the standard mode, which is used for general measurements of visibility, the high range mode, which is used for measurements in areas with very low visibility, and the low range mode, which is used for measurements in areas with high

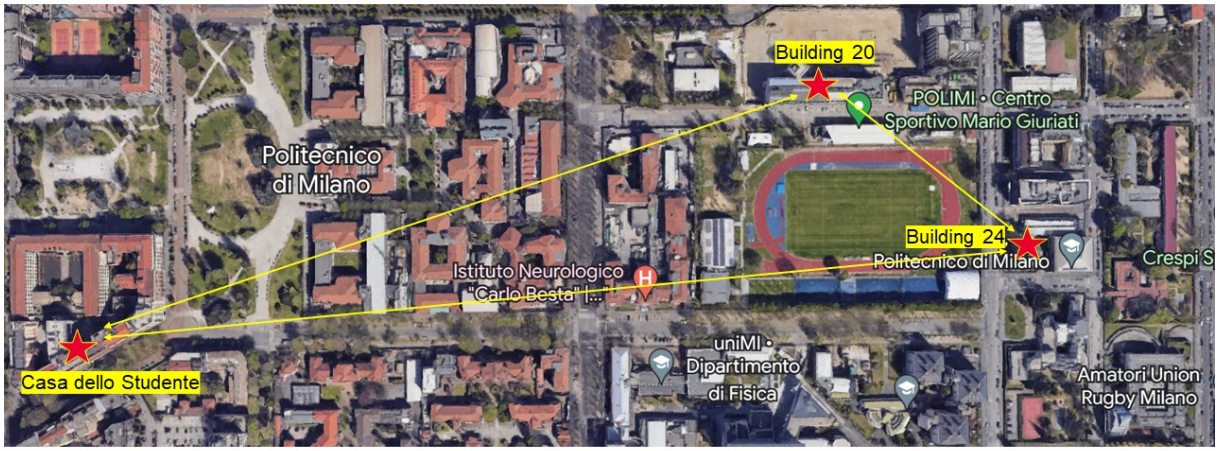

Figure 2.4: View from satellite of POLIMI buildings [11]

visibility. It also has a built-in calculator which can be used to calculate visibility based on the measurements taken.
The PWD20 is a reliable and accurate instrument for measuring visibility and aerosol concentrations in the atmosphere. It is used by researchers, meteorologists and air quality professionals to evaluate and monitor visibility and air quality [25].
Visibilimeters data are sampled every 15 seconds, this means that for a minute of data we have 4 samples. The data have been processed imposing a saturation value (10 km) and the same time stamps have been calculated in order to have the maximum accuracy between the three considered locations.
Building 20 (B20) has a different visibilimeter manufactured by Campbell. The plot in Fig.2.6 shows the trend of the visibility values. It is clear the similarity between the red (CdS) and the green (B24) curves which come from the same kind of instrument. Data collected go from August 2022 up to January 2023. The main role of this data is to make possible a reliable comparison between the estimated data (ECMWF) and the measured one. These data will also be used for the prediction of our correlation coefficient (Chapter3).

Figure 2.5: Vaisala PWD20 Visibilimeter

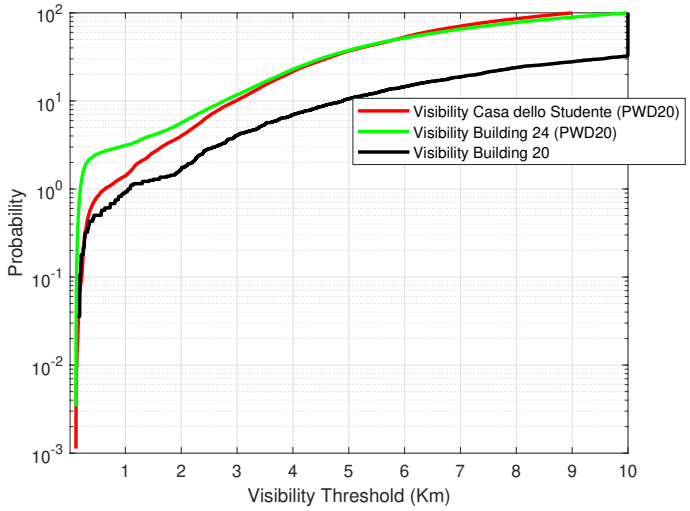

Figure 2.6: CDF comparison between B24,B20 and Casa dello Studente

2.3.2. Milano Linate, Cagliari and Palermo Airport

This section is dedicated to the analysis of the three locations obtained through the NOAA (The National Oceanic and Atmospheric Administration) [23] database available at University of Wyoming Repository[24]. In the following chapter we are going to call this set of data as "repository". Surface data are collected in airports worldwide. The data collected are near by airport due to the presence of visibility phenomena which are object of study in such kind of locations. The data sampling time is 30 or 60 minutes and they are available from 1997 until 2021. For our purpose we considered only the data set belonging to 2021 year. The repository not only has visibility information but also temperature, pressure, dew point and so on [21]. A first representation of this analysis is

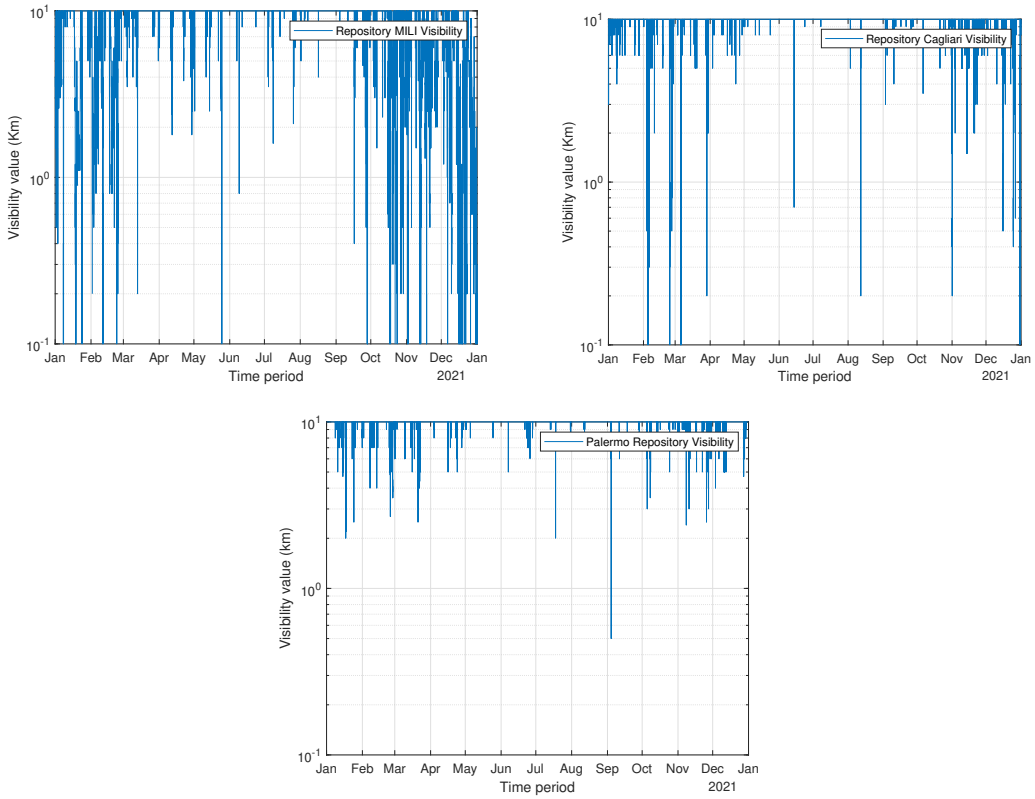

Figure 2.7: Temporal series of MILI, Cagliari and Palermo data

shown in the time series in Fig.2.7.

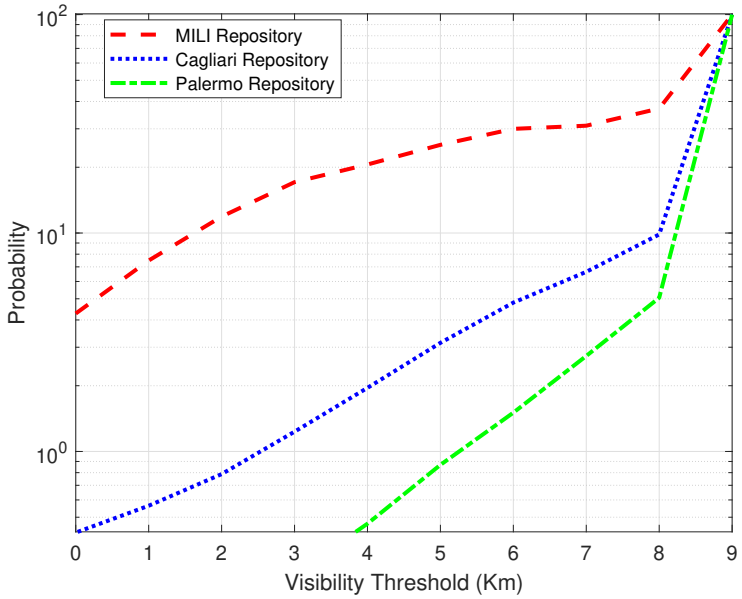

Figure 2.8: CDF of MILI, Cagliari and Palermo from repository data

The same procedure made on ECWMF data has been iterated on this data. The values go from 0 up to 10 km. The best way to visualize our data is through the CDF (Cumulative Distribution Function) in Fig.2.8. Data presents a rough quantization observable by looking at the shape of the three CDFs. These data have been used for the comparison that will be examined in the next section.

2.4. Accuracy of ECMWF Data with respect to the Visibilimeter and Wyoming Repository

Data obtained from ECMWF need to be validated by means of a comparison with the measured one. We are assuming that our data from the visibilimeter and other repositories are reliable enough. This results will be useful in the comprehension of how much is accurate the forecasting prediction of ECMWF. The pixel used for this purpose is one for each location and it has been chosen comparing the most similar ECWMF pixel to the repository one.

We are going to use a mathematical approach which regards the so called Root Mean Square Error (RMSE). RMSE will be used in comparison between visibility and attenuation of the three main locations of repository with respect to ECMWF. ECMWF is a universal database, it is worldwide. If one could prove its accuracy, we would have a global database for fog data to feed into the model that estimates attenuation. Thus now we will test how accurate it is.

RMSE is a valid scoring rule that is easy to comprehend and works with some of the most general statistical suppositions. Root mean square error or root mean square deviation is one of the most widely used metrics for assessing the accuracy of predictions. It quantifies the distance between predicted values and true values using Euclidean distance.

In order to calculate RMSE, work out the residual (difference between prediction and reality) for each data point, calculate the norm of residual for each data point, take the average of residuals and take the square root of that average. RMSE is commonly used in supervised learning applications, as RMSE requires and utilizes true measurements at each predicted data point [9]. This is commonly expressed as follow:

$$RMSE = \sqrt{\sum_{i=1}^{N} \frac{(\hat{y}_i - y_i)^2}{n}} \tag{2.7}$$

where:

- $\hat{y}_i$ is the actual observation time series

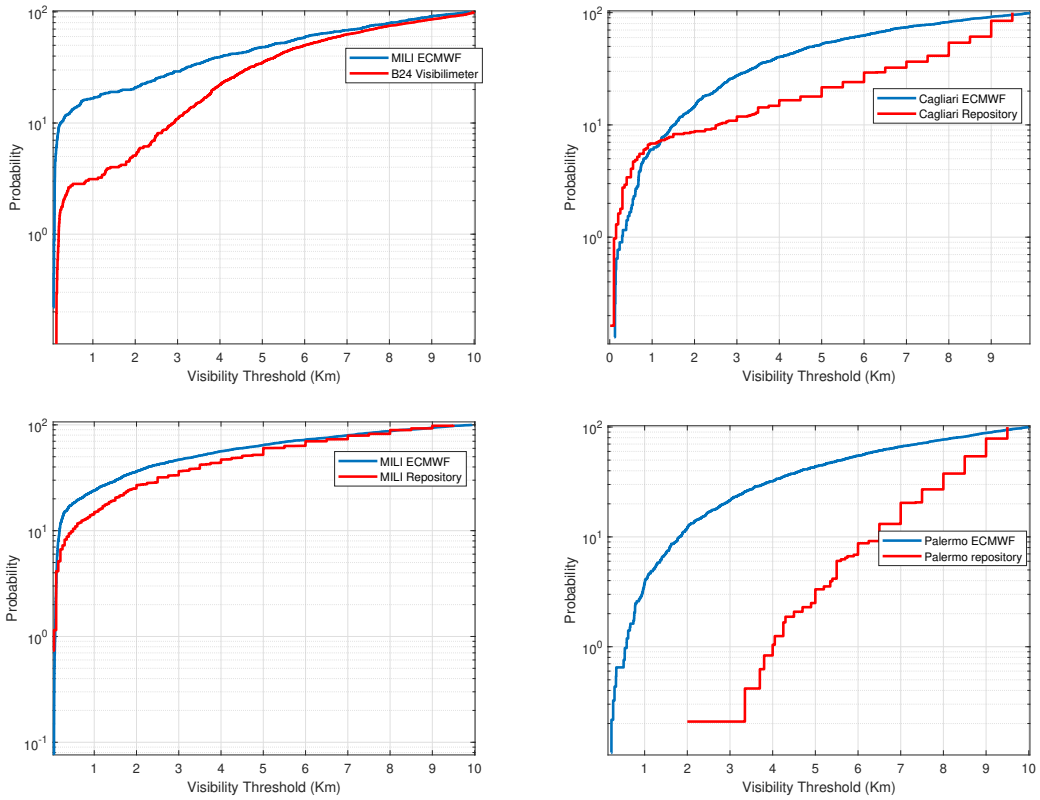

Figure 2.9: Comparison between Visibility CDF of ECMWF and Visibilimeter/Repository

- y_i is the estimated time series
- n is the number of non-missing data points

RMSE on Visibility

As already mentioned this calculations were made to understand which is the error between the predicted data (ECMWF) with the the observed one (Visibilimeter and Repository). Here we are going to enumerate each passage made on the data in order to obtain the wanted result:

1. Selected the set of data belonging to ECMWF which we want to compare with Visibilimeter or repository data Time stamps of the two databases are different. The same period was selected. The data is saturated at a threshold of 10 km
2. Plot the CDF of each dataset (Fig.2.9)

3. Set the same Y axis (Probability axis goes from 0 up to 100%) and interpolate the X (Visibility value) axis of the two CDFs
4. Make the difference between the new CDFs of each pixel , but now they will have same Y axis and different X axis, thus we obtain the RMSE as function of visibility

Looking at the plots in Fig.2.9 we can appreciate the visible difference between some curves (i.e. Palermo ECMWF vs Palermo repository) which can be translated in a large RMSE. Each RMSE is summarized in Table2.1. The best result obtained regards Milano Linate compared with the repository. Cagliari and Palermo can be considered really far from the expected result. Thus, in terms of visibility we can conclude that ECMWF does not guarantee always a reliable data set. It is influenced by the considered location.

Locations	**RMSE**
MILI w.r.t. B24 Visibilimeter	1.33 km
MILI w.r.t. repository	0.7538 km
Palermo w.r.t. repository	2.948 km
Cagliari w.r.t. repository	2.23 km

Table 2.1: RMSE Value Based on Visibility

RMSE on Attenuation

RMSE procedure can be implemented for attenuation due to visibility, as well. Attenuation will be our focus in the next chapters and it is the main source of impairements in FSO links. If we are able to detect it we can also study its variability with respect to the Visibilimeter and repositry. The procedure is quite similar to the past enumerated:

1. Selected the set of data belonging to ECMWF which we want to compare with Visibilimeter or repository data
2. We transform the visibility into attenuation according to KIM model [22]:
3. Time stamps of the two databases are different. The same period was selected. The data is saturated at a threshold of 10 km
4. Plot the CDFs of each dataset (Fig.2.9)
5. Set the same Y axis (Probability axis goes from 0 up to 100%) and interpolate the X (Attenuation value) axis of the two CDFs
6. Make the difference between the new CDFs of each pixel , but now they will have same Y axis and different X axis, thus we obtain the RMSE as function of Attenu-

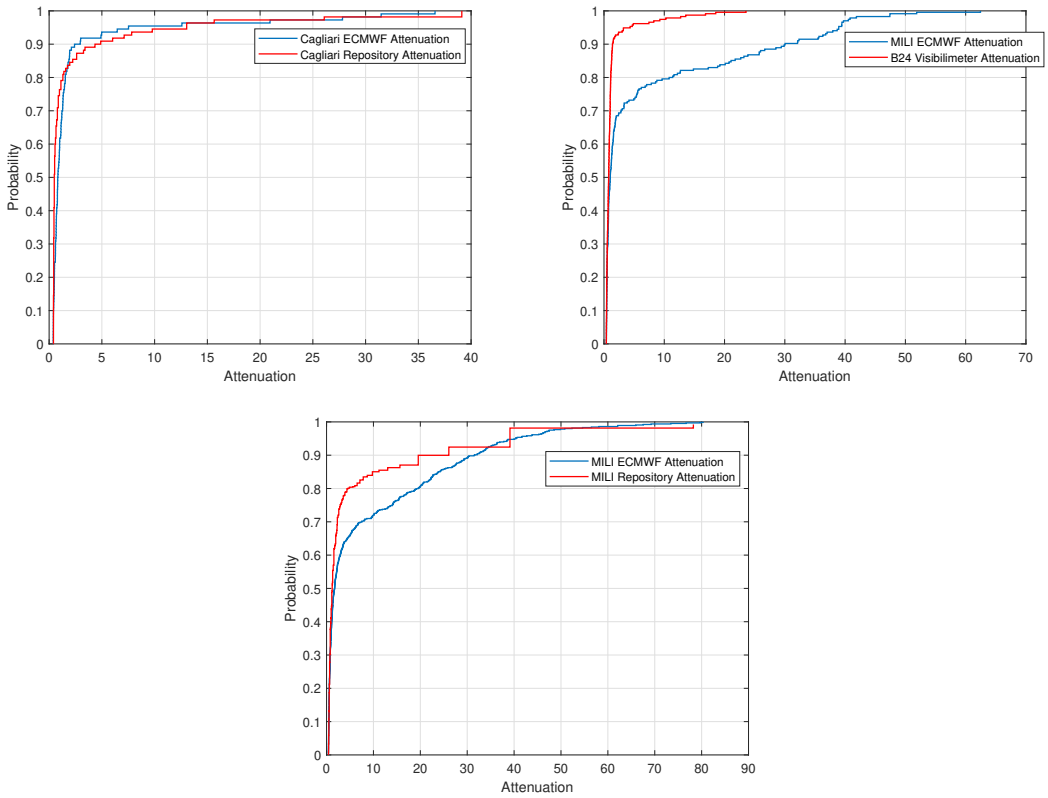

Figure 2.10: Comparison between Attenuation [Np] CDF of ECMWF and Visibilimeter

ation

Results are summarized in Table2.2. According to the obtained results in terms of Attenuation we found a similarity in the two data set considered.

Locations	**RMSE**
MILI w.r.t. B24 Visibilimeter	32.3854 Np
MILI w.r.t. repository	11.3481 Np
Cagliari w.r.t. repository	2.9095 Np

Table 2.2: RMSE Value Based on Attenuation

3 | Model for the Attenuation due to visibility

Visibility was initially formulated for meteorological purposes as a quantity to be calculated by a human witness, and observations made in such a way are extensively utilized. Nevertheless, the estimation of visibility is impacted by numerous subjective and physical aspects. In this chapter we are going to address several topics concerning visibility from a physical point of view. First of all, we are going to analyse the statistical model of this phenomenon, looking for a statistical distribution that can come as close as possible to the fog phenomenon. The same will be done for the attenuation due to visibility. We will then analyse the spatial correlation that our data may assume, divided by location and period. Finally, a new model for estimating attenuation using a new correction factor will be introduced.

3.1. Statistic of visibility phenomenon

It is possible to assume a specific trend about visibility strictly related to the location where it is analysed and the period when it is measured. In this research different locations have been analysed such as Milano, Cagliari and Palermo. Each one of them have a different visibility behaviour due to the different climate and scenarios. Milano is a huge town bordering at north with Alps while in the south we have the Po valley which both involve various visibility demeanor. Cagliari and Palermo are coastal cities in addition due to this feature and recalling the definition of fog, i.e. it forms when moist air cools to the point of condensation, and this occurs more easily in temperate climates, such as coastal areas.

An effective method to compare visibility measurements is to deal with the statistic of this phenomenon.

From a spatial point of view the pixel grid (ECMWF) for some locations such as Palermo and Cagliari has been separated into coastal environment and hinterland one. As shown in Fig.2.1 we introduced a distinction between the two areas. The same has been done

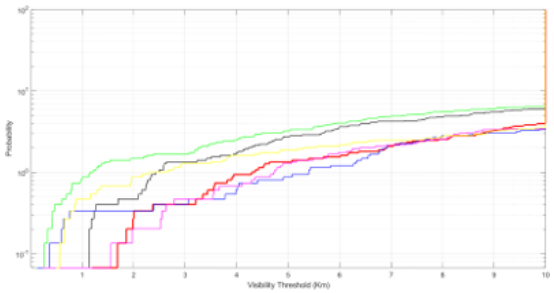

Figure 3.1: Summer season in Palermo coastal

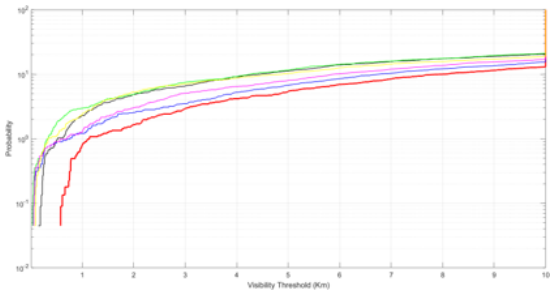

Figure 3.2: Winter season in Palermo coastal

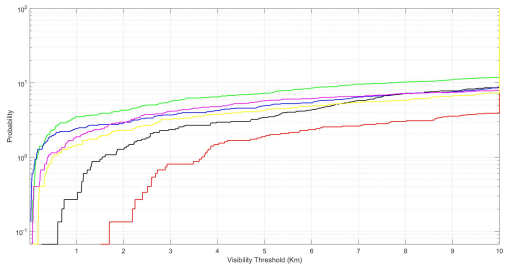

Figure 3.3: Summer season in Palermo Hinterland

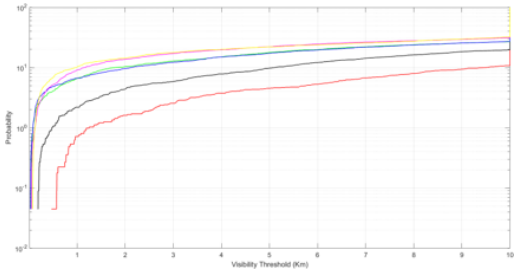

Figure 3.4: Winter season in Palermo Hinterland

for Cagliari, for which we can assume about the same trend of visibility such for Palermo. Plots in Fig.3.1,3.2,3.3,3.4 synthesize the visibility difference between coastal and hinterland environment: we analyse the period dividing the data time into the two main season: Winter and Summer. The meteorological winter begins on 1 December and ends on 28 February, lasting exactly 90 days. Summer is the warmest time of the year, as opposed to winter, which is seen as the coldest. In this sense, the season runs from 1 June to 31 August. For hinterland and city plots we did not consider the spring and autumn. In Fig.3.7 is shown which pixels are considered hinterland (red) and coastal(blue). From the graphs we can appreciate the different trends of our CDF, where we can notice that for lower visibility threshold the winter season has higher probability, as expected. Each pixel considered in the plots 3.1,3.2,3.3,3.4 has a different color and has been chosen among the triangle marked in the Fig.2.1. The distribution of CDF visibility in seacost pixels seems to be more homogeneous than in terrestrial pixels, where we can appreciate a clear distinction between the various pixel examined. The same study has been conducted for Milano, where we distinguished between the rural and urban area. The comprehension of this two different environments will be helpful for understanding the next calculation. In the Fig.3.5,3.6 is shown the statistic of visibility for Milano.

In this preliminary analysis the visibility variability due to the environment is shown.

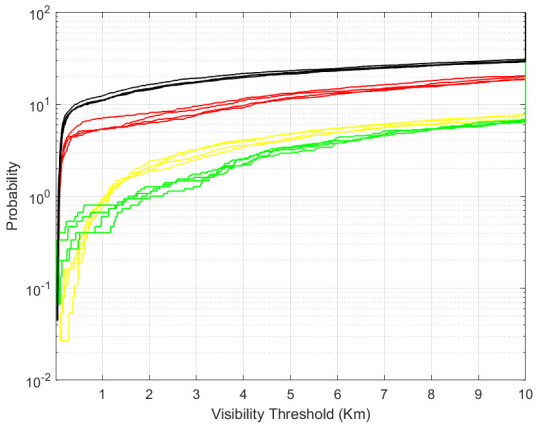

Figure 3.5: Milano rural area. BLACK: Winter, RED: Autumn, GREEN: Summer, YELLOW: Spring

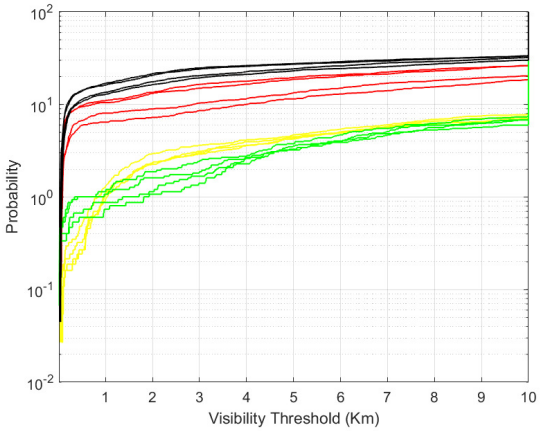

Figure 3.6: Milano urban area. BLACK: Winter, RED: Autumn, GREEN: Summer, YELLOW: Spring

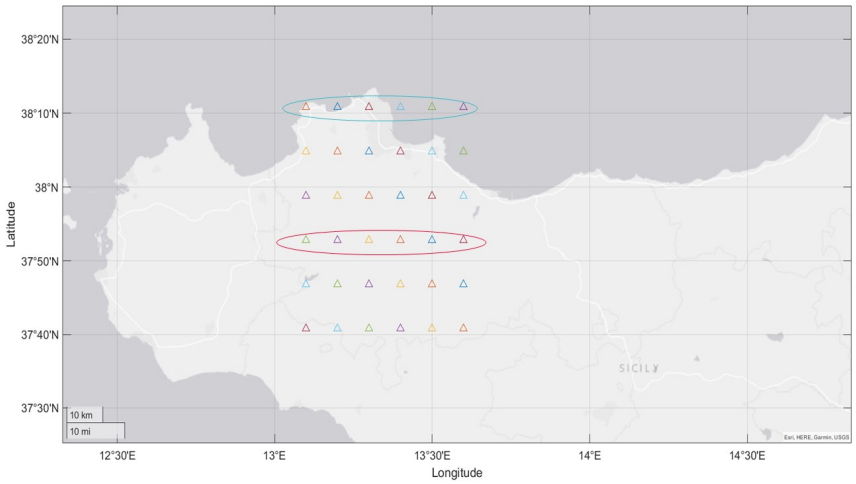

Figure 3.7: Palermo coastal(blue circle) and hinterland(red circle) pixel

There are other possible behaviour associated to other environments such as the tropical or the northern countries.

3.2. Attenuation Model of Visibility

In this section we will focus on how visibility attenuation can be described. We adopted a visibility transformation, chosen to allow better statistical modelling of V, described by this formula:

$$A = -log_{10}V \tag{3.1}$$

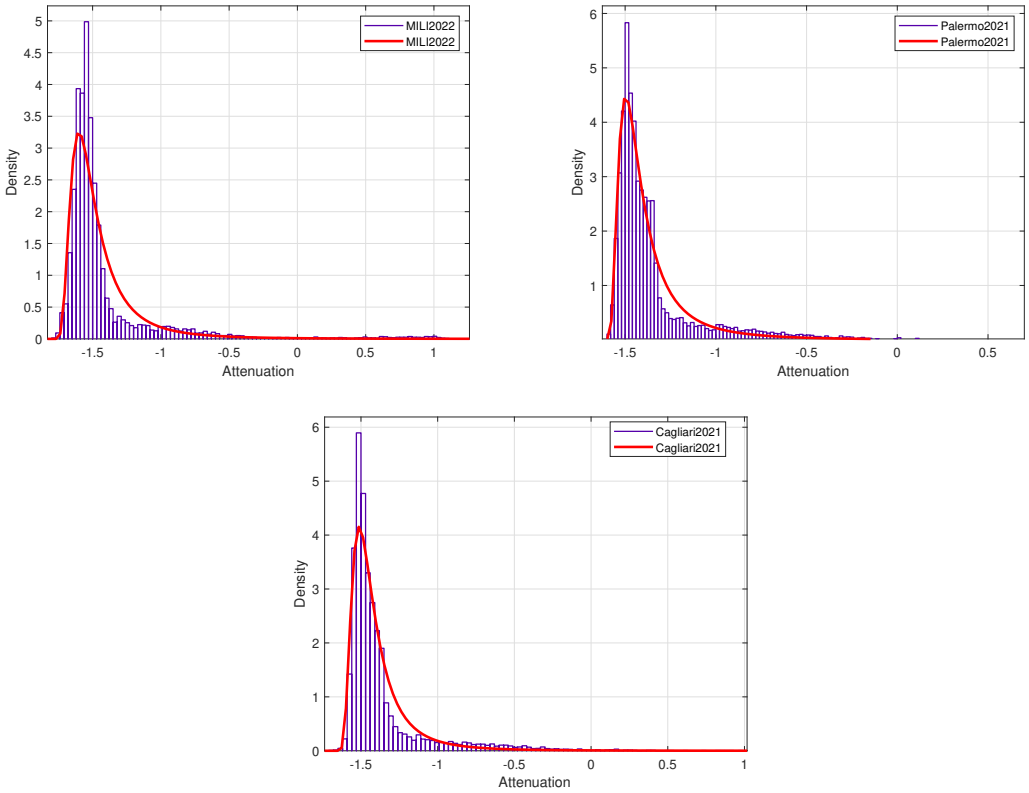

Figure 3.8: Probability Density Function of Attenuation distribution

where V is the visibility in km.

From a statistical point of view we found an interesting function model which approximately describes this event and it is called " Generalized Extreme Value distribution". The generalized extreme value distribution is regularly employed to model the minimum or maximum value among a big collection of independent, similarly distributed random values reflecting measurements or observations. The generalized extreme value combines three plainer distributions into one form, permitting a continuous range of possible shapes that contains all three of the plainer distributions. The distribution used can be represented by a few parameters, which makes it useful in describing this attenuation[3].

The probability density function for the generalized extreme value distribution with location parameter μ, scale parameter σ, and shape parameter $k \neq 0$ is:

$$y = f(x|k,\mu,\sigma) = \frac{1}{\sigma}\exp -((1+k\frac{(x-\mu)}{\sigma})^{\frac{-1}{k}})(1+k\frac{(x-\mu)}{\sigma})^{-1-\frac{1}{k}} \tag{3.2}$$

for

$$1+k\frac{(x-\mu)}{\sigma} > 0 \tag{3.3}$$

The result of this model is shown in Fig.3.8 application, the blue rectangles represents

Table 3.1: Parameters for Generalized Extreme Value distribution

Location	k	σ	μ
MILI 2022	0.35	0.11	-1.56
Cagliari 2021	0.33	0.09	-1.48
Palermo 2021	0.46	0.09	-1.46

the PDF of our data while the red curve is the model approximation. For a better comprehension numerical results are shown in Table 3.1, where we can notice that the three distribution parameters are really similar in value each other.

3.3. Spatial Correlation

Visibility observations taken in different places may not be independent. For instance, readings made in close proximity could be nearer in value than those taken in more distant locations. This is known as spatial correlation indicated in the following paragraph as ρ. Spatial correlation assesses the correlation of a parameter with itself across space. Spatial correlation can be either positive or negative. Positive spatial correlation close to 1 indicates that the two locations considered may have same trend over time. Negative spatial correlation close to -1 implies that there is a low correspondence between the two analysed data set.
The statistical operators required for this calculation are the mean value and the standard deviation of our data which are defined as follow ,where X is our random variable. The expected value $\mathbb{E}[X]$ is the arithmetic mean of a large number of independently selected outcomes of a random variable:

$$\mathbb{E}[X] = \sum_k x_k P(X = x_k) \tag{3.4}$$

The variance can be considered a synthetic measure of the deviation of X from its average value. The root σ_x of the variance is called the standard deviation or deviation mean square and is expressed in this way, where m_{kX} is our momentum:

$$\sigma_X^2 = \mathbb{E}[(X - m_X)^2] = \mathbb{E}[X^2] - 2\mathbb{E}[X]m_X + m_X^2 = \mathbb{E}[X^2] - m_X^2 \tag{3.5}$$

The following formula explains which quantities are applied for our goal [7]:

$$\rho_s(j_1, j_2) = \frac{\mathbb{E}[R_s(j_1, t) \cdot R_s(j_2, t)] - \mathbb{E}[R_s(j_1, t)] \cdot \mathbb{E}[R_s(j_2, t)]}{\sigma[R_s(j_1, t)]\sigma[R_s(j_2, t)]} \tag{3.6}$$

Here the steps made to obtain our correlation value are explained in detail [18]:

1. Suppose to set and lock the pixel j_1 as the first pixel of our grid (6x6 pixel of ECMWF data) and take the time series value R_s.
2. The pixel j_2 is selected among one of the other 35 remaining pixels.
3. The aforesaid matrix has been correlated with the distance of each pixel from another one.
4. Afterwards each group of correlation coefficients belonging to a specific pixel have been stored in a matrix.
5. Restart locking j_1 as the second pixel of our grid and repeat the steps... .

The first graph in Fig.3.9 gives us the evaluation of how much the correlation value is spread along the pixels and how much it changes between the pixels. The colored circles represent the correlation value as combination of each couple of pixels in the ECMEF grid, while the red line is the average value as function of distance. We can notice that for each distance of the grid we have a massive number of samples. A neater way to visualize the result of the red line is shown in Fig.3.11, the average line is plotted for Cagliari and Palermo as well. Here the path followed by the red line is highlined by the scatter points in Fig.3.11.
Pixels from ECMWF are 10 km apart from each other, thus the measurements needed an intermediate point which could cover small distances in the curve approximation. Regarding Milano two more points have been added in the calculation of the spatial correlation. This correlation coefficients is calculated from the visibilimeter's measurements: "Building 24" (B24) , "Building 20" (B20) and "Casa dello Studente" (CdS) respectively. Correlation values are: $\rho_{B20-CdS} = 0.9615$ while $\rho_{B24-CdS} = 0.9759$ and the distance from each locations are $d_{B20-CdS} = 650m$ while $d_{B24-CdS} = 800m$. This points have been added in the calculation in order have a more accurate trend of our fitting curve that will be introduced after. What we can notice right away is that growing in distance with respect to our starting pixel the correlation coefficients start decreasing in value as expected.The correlation is strong in the first 15 km of space while becomes less robust increasing the distance.
Best way to work on this correlation coefficients is to build a robust and effective statistic model fitting ρ. Data sets are fitted with an exponential curve. A form of regression is used to determine the best-fitting exponential equations that describe a set of data. The process of data fitting with an exponential function begins with identifying the model that fits the data best. Then, the best equation to use is sought and parameters are adjusted

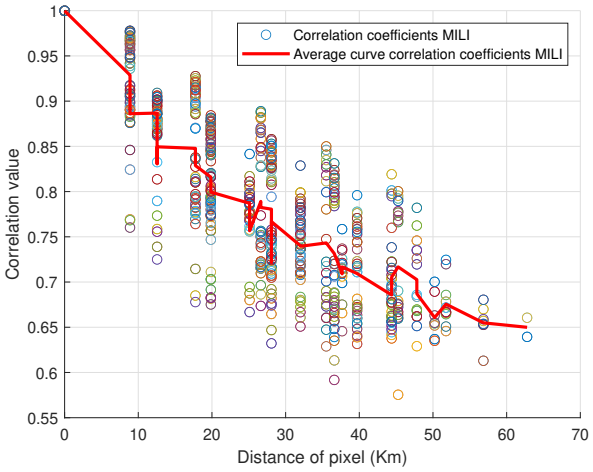

Figure 3.9: Correlation Values for each pixel MILI

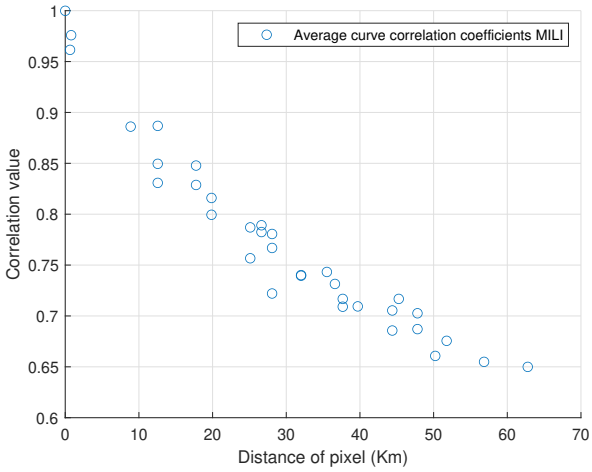

Figure 3.10: Average Correlation Values for each pixel MILI

to achieve the best possible results. Finally, the model is evaluated and the results are compared to the original data [2].
The exponential function used for the fitting is the following:

$$f(x) = ae^{bx} + ce^{dx} + k \tag{3.7}$$

If the coefficient linked to b and/or d is negative, y stands for exponential decay. If the coefficient is positive, y stands for exponential growth. Here there is an additional factor which is k, it represents the constant term, which was introduced to describe particular situation of the correlation values which could be also negative and the exponential function with out this factor would been ineffective against this behaviour due to the nature of this function itself (exponential is always greater than 0).
The result of the aforesaid fitting is shown in Fig.3.12. As mentioned before the correlation coefficient $\rho \in [-1, 1]$ and it is fundamental to set a starting point which coincides with the $\rho = 1$. In order to obtain that condition we faced an optimization task which required some basic concepts of mathematical analysis. The steps made are the following:

1. Set the double exponential equation 3.7 which will fit the data
2. Find and minimize the objective function

$$g_i(x) = |f_i(x) - y_i|^2 \tag{3.8}$$

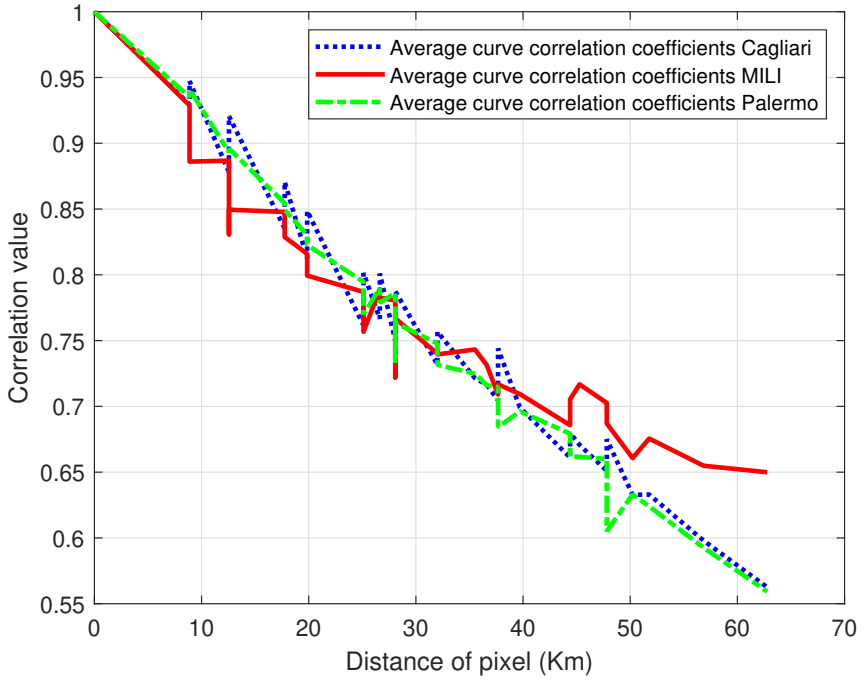

Figure 3.11: Average Correlation Values of ECMWF locations

$$G(x) = \sum_{i=1}^{N} g_i(x) = \sum_{i=1}^{N} |ae^{bx} + ce^{dx} + k - y_i|^2 \tag{3.9}$$

3. Define the constraint: linear

$$f(0) = 1 \tag{3.10}$$

$$f(0) = a + c + k \tag{3.11}$$

Milano Linate dataset covers two years (2021 and 2022) and have been subdivided in two databases. Thus, in order to understand the actual behaviour of ρ and the possible mutation of the visibility during the years, the correlation factor of the two datasets have been compared making the same operation enumerated before. The results are shown in Fig.3.13.

Results are available for the other locations such as Cagliari and Palermo as well. In Fig.3.14 it is possible to appreciate how much the correlation curves are close to each other in the first 15 km. In the Fig.3.15 there is a zoom in order to appreciate the results for the distance from 0 up to 40 km. For our purposes we are going to consider path length never larger than 5 km and our focus will be in this range of distances, due to the physical impairments of the FSO system which would been present at larger distances.

As expected, according to the consideration on statistic of visibility in Chapter 3.1, lo-

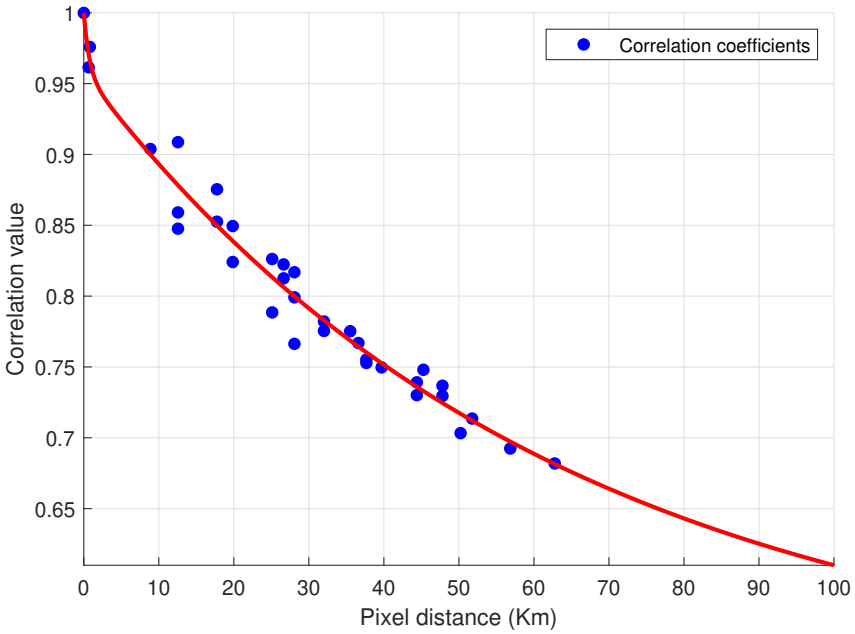

Figure 3.12: MILI fitting model

Fitting coefficients			
Coefficients	**Milano**	**Cagliari**	**Palermo**
a	0.4350	0.6277	0.7011
b	-0.0161	-0.0093	-0.0097
c	0.0423	0.3432	0.2660
d	-1.3429	-0.0094	-0.0097
k	0.5227	0.0291	0.0330

Table 3.2: Fitting coefficients for ECMWF locations

cations which share about the same ecosystem and geographical environment present, in terms of correlation, about the same trend. As matter of fact after 15 km the blue (Palermo) and green (Cagliari) line continue their path which is equal for both, on the other hand the red one (MILI 2021) exceeded the threshold of 15 km starts being less correlated with respect to the other two locations for the reasons listed above. The coefficients needed to calculate the three types of fitting considering the equation 3.7 are listed in Table 3.2:

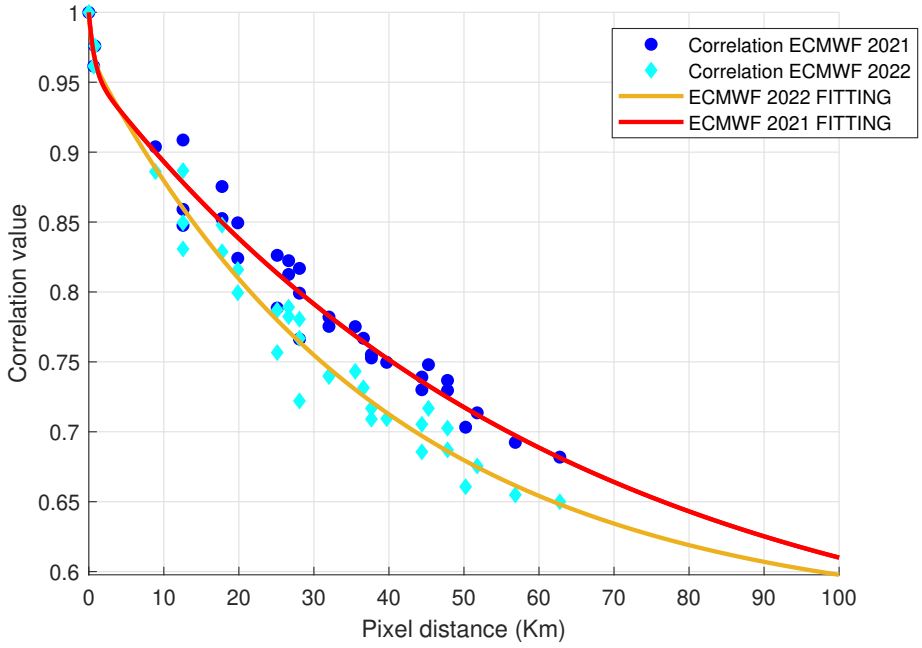

Figure 3.13: MILI 2021 vs MILI 2022 fitting model

3.4. Path Reduction Factor computation

The path reduction factor (PRF) is the main parameter in the prediction model for predicting total attenuation from specific rain attenuation. In literature regarding attenuation due to rain we have many models which explain and evaluate it whereas this study investigates path reduction factor models for the prediction of fog attenuation. The PRF takes into account in an equivalent way the change of the visibility along the path with respect to the value measured at the transmitter or receiver site. It can happen that for a long (i.e. 2 km) link the meteorological phenomenon of fog is not homogeneous. This in-homogeneity can be translated in an effective path through the PRF, which take into account the effect of fog variations along the propagation path [21].

3.4.1. Bulding 24 and Casa dello studente analysis

In our case we are going to analyse a PRF for ECMWF data set and the visibilimeters database: Building 24(B24), Building 20 (B20) and Casa dello Studente (CdS). Starting from this latter we are going to describe in detail each passage made to obtain our result. The meaning of this method is shown in Fig.3.16:

1. Suppose to describe the visibility as a linear interpolation between the starting point (B24) and the final one (CdS)

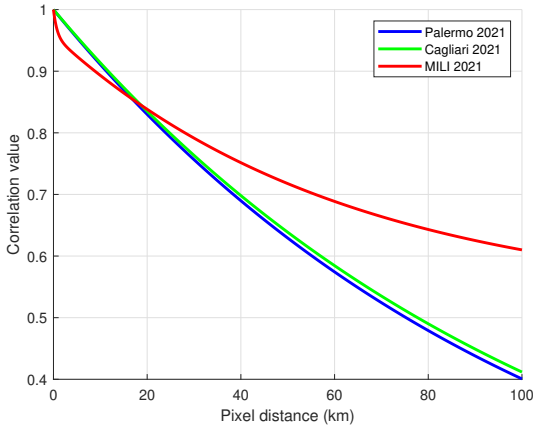

Figure 3.14: MILI, Cagliari and Palermo 2021 fitting models, range 1-100 km

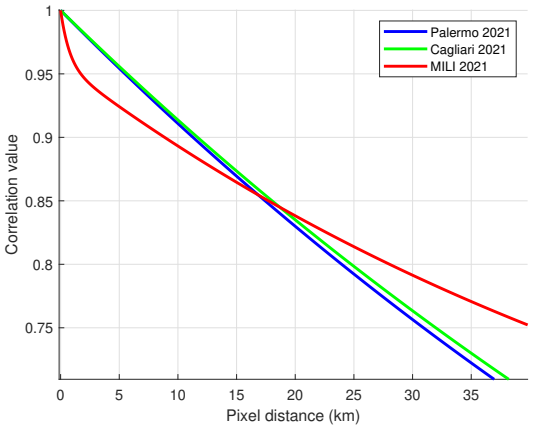

Figure 3.15: MILI, Cagliari and Palermo 2021 fitting models, range 1-40 km

2. Define the metric for the experiment: Path Length = 800 m, the Path Sample ΔL = 10 m or rather how often to calculate the visibility sample along the path
3. For each ΔL calculate the specific attenuation, using the KIM model starting from the sampled V value[22].
4. Afterwards sum up all the specific attenuation α_i from each ΔL for each class N of the link, finding the link's attenuation

$$A_{tot} = \sum_{i=1}^{N} \alpha_i \cdot \Delta L \tag{3.12}$$

5. At this point we have calculated the Attenuation along the path where α is calculated from the initial or final link value in order to reproduce the classic situation where there is only one instrument per link. We can express it as:

$$A_{tot} = \alpha \cdot L \cdot PRF \tag{3.13}$$

6. Inverting the above formula we can extrapolate the PRF, reminding that α in this case is the specific attenuation due to the first value of visibility in the considered starting point

$$PRF = \frac{A_{tot}}{\alpha \cdot L} \tag{3.14}$$

The aforementioned method has been used to calculate our PRF for the link B24-CdS but also for the ECMWF locations such as Milano, Cagliari and Palermo.

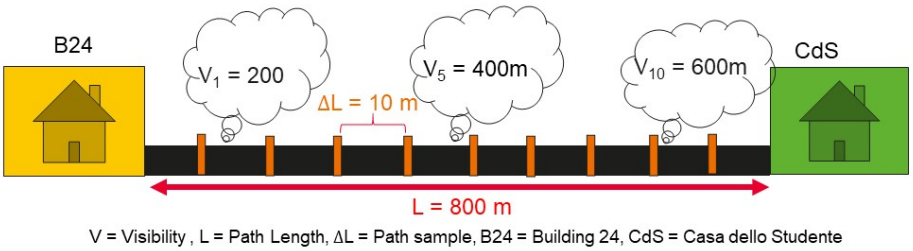

Figure 3.16: Schematic procedure for PRF calculation

The PRF trends as function of visibility are reported in Fig.3.17 and Fig.3.18. In the above mentioned figures, several factors are taken into account. All V values of the time series are used, the data refer to the two contiguous visibilimeters pixels that are 800m apart. Finally, the individual values give many points and from these the density plot was calculated with the various intensity colours according to the number of samples for each site. In this calculation has been included a class of visibility for each PRF, the class is 500 m. Each 500m of visibility value we obtain a correspondent PRF and this step has been done for 20 classes due to the maximum value of visibility available of 10 km. The black pixels in the figures represent the available sample for each value, more black it is more samples are available in this range of visibility. The fundamental purpose of this calculation is shown in the PRF comparison between the B24 and CdS. The two curves shown in Fig.3.17,3.18 were placed in Fig.3.19 in order to make a reasonable comparison. In this figure a sharp change of the PRF in the first 2 km of visibility with two opposite trends is shown. If we consider the Building 24 as far away from the city centre we can observe the high values that PRF assumes. This behaviour is not strange since it is well known that fog is much concentrated in open areas and far away from city centers. According to the blue curve we can estimate an high Path Reduction Factor if we move take the visibility values belonging to the city center or vice versa outside the city. In fact the green line which represents the Building 24 has the opposite behaviour in the first 2 km of visibility with respect to Casa dello Studente. For values of visibility

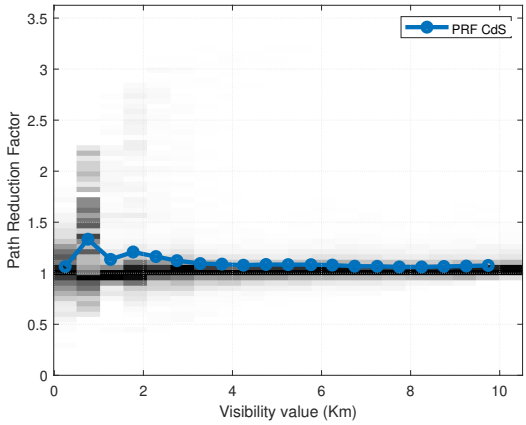

Figure 3.17: PRF density plot for Casa dello Studente

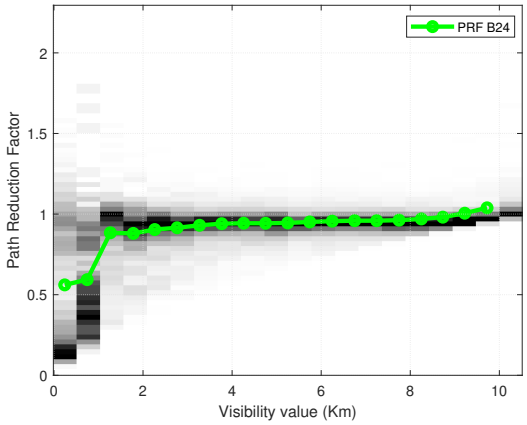

Figure 3.18: PRF density plot for Building 24

higher than 2 km the PRF seems to normalize around 1 which means that low visibility values affect the link in a more incisive way. An effective way to analyse our PRF and understand how much it improves the attenuation estimation on the link is to compare the link's attenuation with the total attenuation. The attenuation curve considering the PRF=1 (thus, not considering it in the calculation) is shown in Fig.3.21 , reminding that PRF is a function of the site where the V is used:
An assumption that must be clear is that a typical FSO system works under 30 dB of margin, higher values of attenuation makes not possible the communication between transmitter and receiver as consequence our focus will be on attenuation value not higher than 50 dB, otherwise higher values would been useless to study anyway. We can appreciate the total attenuation of our link by means of CCDF in Fig.3.20, as matter of fact the two CCDFs are equal, because both curves are derived with the same equation. The blue curve consider the visibility value of B24 while the red one of CdS, this is the only one difference.
In Fig.3.21 is clear the role of the Path Reduction Factor. Starting from the black dash-dot line which represents the attenuation curve of B24 with a PRF which is equal to 1. In order to obtain this result we have manipulated the following formula imposing PRF = 1:

$$A_{tot} = \alpha \cdot L \tag{3.15}$$

The grey dash-dot line is the attenuation regarding CdS with PRF = 1. Thus, grey and black curves simulates the worst case for the link attenuation because they do not consider the PRF introducing a considerable error. This error can be seen comparing the curves with PRF = 1 to the red and blue curves which represents the total attenuation on the

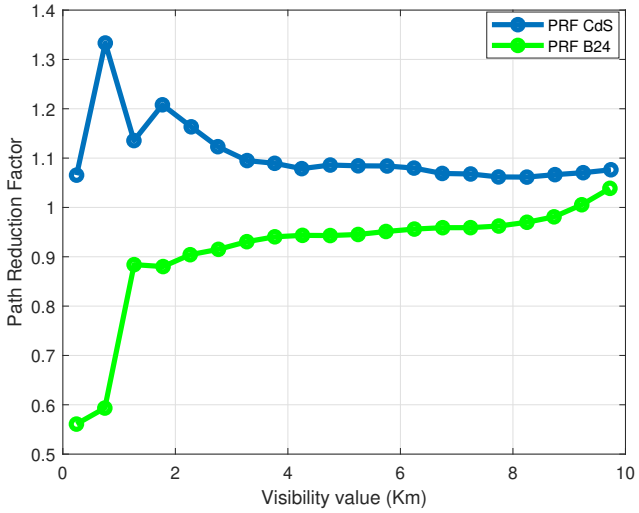

Figure 3.19: B24 vs CdS PRF

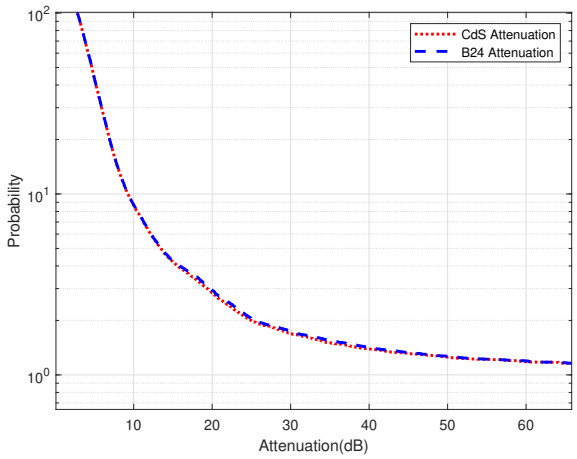

Figure 3.20: B24 and CdS real attenuation

link. Let us turn instead to the curves where PRF is considered. Still focusing on Fig.3.21 the B24 curve (azure) was calculated taking into account the PRF values calculated in the plot 3.19. The same was done for the CdS curve (green). What tell us that PRF improved the attenuation approximation (at least in the first 30 dB of margin) is the proximity of the blue and green curve to the original curves of Fig.3.20.

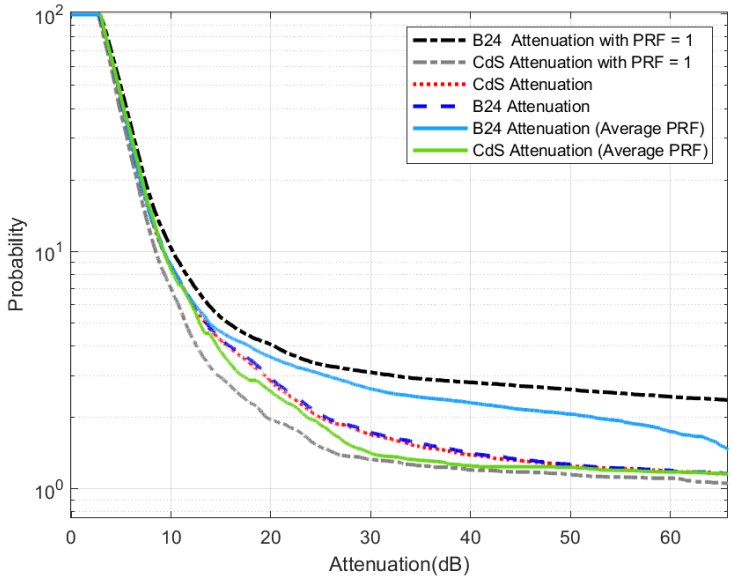

Figure 3.21: Comparison between different PRF values

3.4.2. Milano, Cagliari and Palermo analysis

Same steps were made on ECMWF data set. In this case the comparison is between pixels which are spaced between hinterland and city for MILI and coastal and hinterland for Cagliari and Palermo. The pixel distance is about 10 km. Proceeding on MILI, the results are shown in Fig.3.22. In these figures we have taken 2 pixels which respected the city - hinterland condition. The blue line in figure represents the pixel in city, it is supposed to be the pixel which links the city to the hinterland, same story for the red curve but opposite path, from hinterland to town. Taking into account this consideration we can notice a clear trend for our PRF in the first 2 km of visibility, from the pixel city the blue curve has an high crest which corresponds to an high PRF going to decrease and stabilize around 1, opposite situation for the red line, which represents the link where visibility belongs to hinterland pixel, where it is supposed to have situations where visibility is very low and as consequence the PRF value in the first 2 km are very low. This trend has been discovered in the past paragraph for B24-CdS and for the ECMWF pixels.
From the red and blue curves we have extrapolated the average value for each one of them in order to give a model for the PRF. Focusing on top left of Fig.3.23, the two trends described in the past sections reappear, the purple dot line refers to the city model while the black one refers to the hinterland.
The behaviour of our PRF for Cagliari and Palermo is different. Focusing on the relative figures we can notice that the trend seen for Milano here is not the same, on the contrary

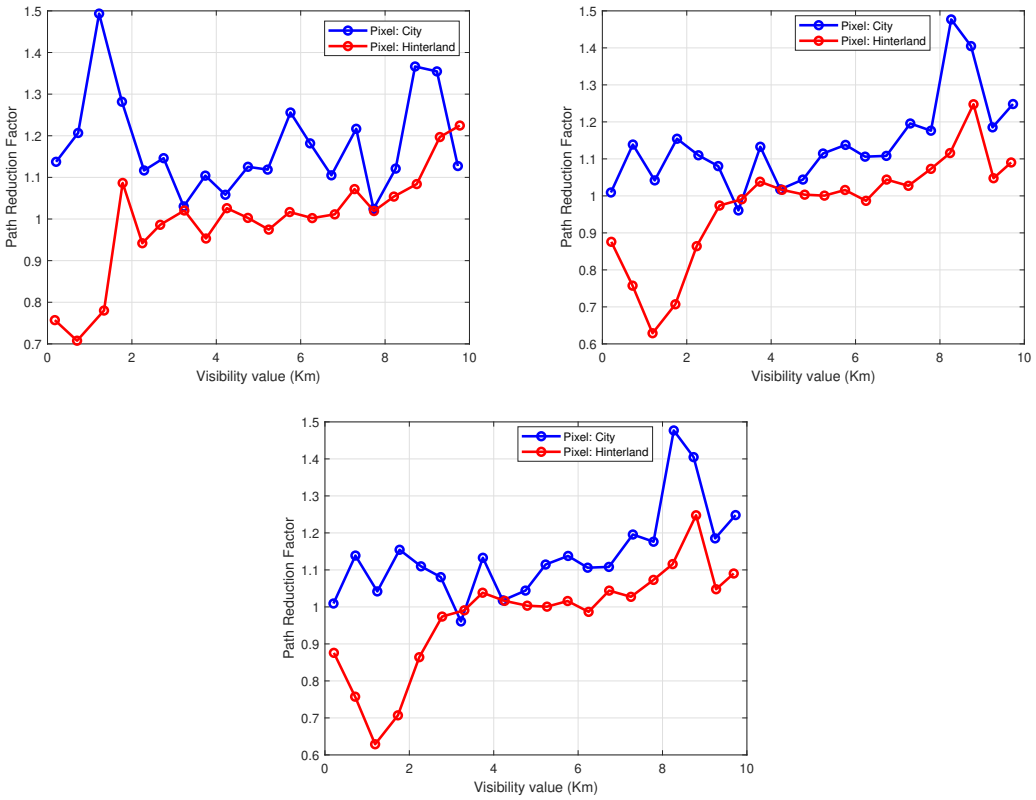

Figure 3.22: MILI PRF city and hinterland comparison

the PRF of hinterland with respect to coastal seems to be scaled of a factor, the comparison between Cagliari and Palermo can be done due to the geographical characteristics that both territories have. As consequence, it was found that the choice of which PRF to apply depends on the geographical area and which V is taken as a reference, i.e. which side of the link.

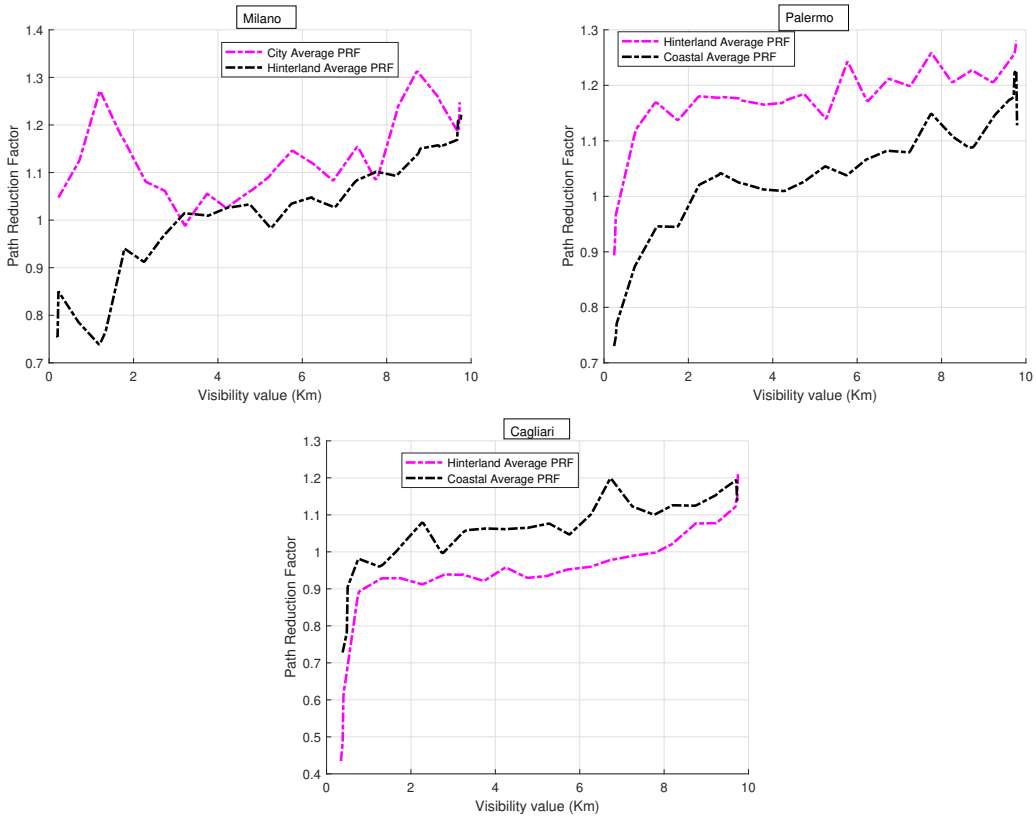

Figure 3.23: PRF comparison between ECMWF locations

4 | Conclusions and future developments

Free Space Optics (FSO) is a powerful technology which makes possible a new kind of communication without giving up on all the benefits of fiber. With such technology that works with the transmission of photons and thus light, atmospheric impairments must be taken into account.
As far as we know visibility is an interesting phenomenon which need our focus in order to discover its peculiarities. From a physical point of view we noticed that visibility is strongly seasonal influenced. In addition climate and locality morphology are not avoidable in this analysis indeed they play an important role. It is obvious that Cagliari and Palermo ECMWF data show a similar trend due to the same climate and seacoasts environment. One cannot say the same for MILI in comparison with them, different trend and characteristics.
Taking advantage of this physical proprierties of visibility, for each locations we tried to generalize in some way this latter. First of all we have identified three different databases which gave us the data of same locations to be analysed: ECMWF, Wyoming and Visibilimeter. Next, we made an accurate comparison of ECMWF data with the other two databases considered by means of the Root Mean Square Error (RMSE). What we noticed is that ECMWF reliability is strongly influenced by the considered location. For some locations it well approximates the visibility data than a visibilimeter or a certificated repository such Wyoming. Regarding the statistical generalization, it has been made by means of a statistical distribution (Generalized Extreme Value) for both visibility and attenuation. The result of this generalization is quite similar to the original Probability Density Function. The final answer to the starting question regarding the ECMWF database and its possibility to be an effective way to analyse and study visibility is still an open question. We need much more observations and comparable locations in order to answer the question precisely.
Subject of studies has been the correlation coefficient which helped us to interpret the visibility evolution along different path at different distances. Values of the correlation

coefficient highlights the strong correlation of the examined pixel. Values near 1 were in the first 15 km of distance between pixels of the same ECMWF grid. Therefore, growing in distance we have a decrease of the correlation coefficient. We can definitely assume that the correlation coefficient behaves inversely with respect to distance.
We analysed different models in literature which regarded attenuation due to rain and fog, specifically. There is a lack of standardization in FSO society which should be balanced with respect to the other systems which works in mm-Wave. Thus, this lack gave us the possibility to develop a model for wavelength near the IR which are the most used for FSO. This model uses a specific variable which has been called Path Reduction Factor (PRF). By means of PRF we estimated the attenuation due to visibility for a Link with a path length of 800 meters in Politecnico di Milano. The results obtained were good enough to say that the use of PRF is really helpful in the dimensioning of our link budget. Same work has been done on ECMWF data, discovering similar value of PRF. Moreover, we managed to distinguish different PRF as function of the location analysed distinguishing between city, hinterland and coastal environment.
In conclusion, more analysis could be done regarding visibility and its attenuation on FSO systems. Thus, a new starting point could be the analysis of temporal correlation of this phenomenon and how it is influenced by spatial correlation. Other investigative leads could be how visibility is influenced by even lower wavelength. The main future development will be the testing of the model for estimating fog attenuation that includes the PRF against the data we are collecting with the experiment in Politecnico di Milano.

Bibliography

[1] Mars - the ecmwf meteorological archive, 2018 2018. URL https://www.ecmwf.int/node/18124.

[2] Exponential models, 2023. URL https://it.mathworks.com/help/curvefit/exponential.html.

[3] Generalized extreme value distribution, 2023. URL https://it.mathworks.com/help/stats/generalized-extreme-value-distribution.html.

[4] Ecmwf official website, 2023. URL https://www.ecmwf.int/.

[5] Mars catalogue details, 2023. URL https://confluence.ecmwf.int/display/UDOC/MARS+content#MARScontent-Atmosphericmodels.

[6] I. Adam Augustyn, Encyclopædia Britannica. Fog definition, 2023. URL https://www.britannica.com/science/fog.

[7] S. Bellini. *Teoria dei fenomeni aleatori*. Esculapio Ingegneria, Via Terracini, 30 - 40131, Bologna, 2012.

[8] S. H. Bloom. The physics of free-space optics. 2001.

[9] c3.ai, 2023. URL https://c3.ai/glossary/data-science/root-mean-square-error-rmse/.

[10] Q. Chen, L. Yang, X. Liu, B. Cheng, J. Guo, and X. Li. Modeling and analysis of inter-satellite link in leo satellite networks. In *2021 13th International Conference on Communication Software and Networks (ICCSN)*, pages 134–138, 2021. doi: 10.1109/ICCSN52437.2021.9463648.

[11] G. Earth, 2023. URL https://earth.google.com/web/.

[12] M. B. L. M. D. F. T. U. d. R. S. F. Bisegna, F. Gugliermetti. Stato dell'arte dei led (light emitting diodes). Technical report, Accordo di Programma Ministero dello Sviluppo Economico – ENEA, 6 2010.

[13] E. C. for Medium-Range Weather Forecasts. *IFS DOCUMENTATION – Cy43r1 - PART IV: PHYSICAL PROCESSES*. European Centre for Medium-Range Weather Forecasts, Shinfield Park, Reading, RG2 9AX, England, 11 2016.

[14] P. Heinz Willebrand and B. S. Ghuman. *Free-Space Optics: Enabling Optical Connectivity in Today's Networks*. Linda Engelman, 800 East 96th St., Indianapolis, Indiana 46240 USA, 2002.

[15] ITU. Prediction methods required for the design of terrestrial free-space optical links, 207. URL `https://www.itu.int/rec/R-REC-P.1814-0-200708-I/en`.

[16] R. L. P. Larry C. Andrews. *Laser Beam Propagation through Random Media, Second Edition*. 2 edition, 2005. ISBN 9780819478320.

[17] Z. Lee and S. Shang. Visibility: How applicable is the century-old koschmieder model? *Journal of the Atmospheric Sciences*, 73(11):4573 – 4581, 2016. doi: 10.1175/JAS-D-16-0102.1. URL `https://journals.ametsoc.org/view/journals/atsc/73/11/jas-d-16-0102.1.xml`.

[18] L. Luini and C. Capsoni. The impact of space and time averaging on the spatial correlation of rainfall. *Radio Science*, 47, 06 2012. doi: 10.1029/2011RS004915.

[19] I. T. P. W. Y. Z. Massimo Tornatore, Biswanath Mukherjee. *Springer Handbook of Optical Networks*. Springer Cham, Gewerbestrasse 11, 6330 Cham, Switzerland, 10 2020. ISBN 978-3-030-16249-8.

[20] E. Matricciani. *Meccanica celeste e orbite dei satelliti*. Esculapio Ingegneria, Via Terracini, 30 - 40131, Bologna, 2012.

[21] C. E. V. MUNOZ. *FOG AND RAIN ATTENUATION MODELS FOR THE DESIGN OF FSO LINKS IN 5G+*. PhD thesis, PONTIFÍCIA UNIVERSIDADE CATÓLICA DO RIO DE JANEIRO - PUC-RIO, Rua Marquês de São Vicente, 225, Gávea - Rio de Janeiro, RJ - Brasil, 8 2022.

[22] R. Nebuloni and E. Verdugo. Fso path loss model based on the visibility. *IEEE Photonics Journal*, 14(2):1–9, 2022. doi: 10.1109/JPHOT.2022.3152728.

[23] N. Oceanic and A. Administration, 2023. URL `https://www.noaa.gov/`.

[24] U. of Wyoming, 2023. URL `https://weather.uwyo.edu/surface/`.

[25] V. Oyj. *Present Weather and Visibility Sensors PWD10, PWD12, PWD20, and PWD22*, 2018.

List of Figures

List of Tables